

## Development of New Three-Dimensional Rock Mass Strength Criteria

Mohammad Hadi Mehranpour<sup>1,2</sup> · Pinnaduwa H. S. W. Kulatilake<sup>1</sup> · Ma Xingen<sup>3</sup> · Manchao He<sup>3</sup>

Received: 7 March 2018 / Accepted: 25 June 2018 / Published online: 30 June 2018

© Springer-Verlag GmbH Austria, part of Springer Nature 2018

### Abstract

Two new three-dimensional rock mass strength criteria are developed in this paper by extending an existing rock mass strength criterion. These criteria incorporate the effects of the intermediate principal stress, minimum principal stress and the anisotropy resulting from these stresses acting on the fracture system. In addition, these criteria have the capability of capturing the anisotropic and scale dependent behavior of the jointed rock mass strength by incorporating the effect of fracture geometry through the fracture tensor components. The new criteria are proposed after analyzing 284 numerical modeling results of the polyaxial, triaxial and biaxial compression tests conducted on the jointed rock blocks having one or two joint sets by the PFC<sup>3D</sup> software. Some of these simulation results were compared with experimental results to validate the developed PFC<sup>3D</sup> model that was used for numerical modeling of jointed blocks. In this research to have several samples with the same properties a synthetic rock material that is made out of a mixture of gypsum, sand and water was used. Altogether, 12 joint systems were chosen; some of them had one joint set and the rest had two joint sets. Joint sets have different dip angles varying from 15° to 45° at an interval of 15° with dip directions of 30° and 75° for the two joint sets. Each joint set also has three persistent joints with the joint spacing of 42 mm in a cubic sample of size 160 mm. The minimum and intermediate principal stress combination values were chosen based on the uniaxial compressive strength (UCS) value of the modeled intact synthetic rock. The minimum principal stress values were chosen as 0, 0.2, 0.4 and 0.6 of the UCS. For each minimum principal stress value, the intermediate principal stress value varies starting at the minimum principal stress value and increasing at an interval of 0.2 of the UCS until it is slightly lower than the strength of the sample under the biaxial loading condition with the same minimum principal stress value. To express the new rock mass strength criteria, it was also necessary to determine the intact rock strengths under the same confining stress combinations mentioned earlier. Therefore, the intact rock was also modeled for all three compression tests and the intact rock strengths were found for 33 different minimum and intermediate principal stress combinations.

**Keywords** Discrete element method (DEM) · Particle flow code (PFC) · Rock mass strength · Polyaxial compression test · Intermediate principal stress · Fracture tensor

### List of Symbols

$A$	Disk area
$a, a_2, a_3, b, b_2, b_3$	Empirical coefficients
$B$	An empirical constant

$B^J$	Constant coefficient of the modified smooth-joint contact model
$C_J$	Joint cohesion
$D_{\min}, D_{\max}$	Minimum and maximum particle diameters
$E_c, \bar{E}_c$	Contact and bond Young's modulus of the linear parallel bond model, respectively
$F_{ij}, F_{ij}^r, F_{ij}^k$	Fracture tensor, fracture tensor of the rock mass and fracture tensor of the $k$ th joint set, respectively
$F_{11}, F_{22}, F_{33}$	Fracture tensor components in the maximum, intermediate and minimum principal stress directions, respectively
$f, f_2, f_3$	Monotonically decreasing functions

✉ Pinnaduwa H. S. W. Kulatilake  
kulatila@u.arizona.edu

<sup>1</sup> Rock Mass Modeling and Computational Rock Mechanics Laboratories, University of Arizona, Tucson, AZ 85721, USA

<sup>2</sup> Present Address: HPT-Laboratory, Faculty of Geosciences, Utrecht University, Utrecht, The Netherlands

<sup>3</sup> State Key Laboratory for Geomechanics and Deep Underground Engineering, China University of Mining and Technology, Beijing, China

		<b>Abbreviations</b>	
$K_n^J, K_s^J$	Joint normal and shear stiffnesses, respectively	CUMTB	China University of Mining and Technology, Beijing
$k_n^J, k_s^J$	Joint normal and shear stiffnesses of the modified smooth-joint contact model, respectively	DEM	Discrete element method
$k_{n_{\min}}^J$	Minimum joint normal stiffness of the modified smooth-joint contact model	JSC	Joint sides checking approach
$k_r, \bar{k}_r$	Ratio of the normal to shear stiffnesses of the contact and bond for the linear parallel bond model, respectively	LPBM	Linear parallel bond model
$m$	Number of parameters to be estimated	LVDT	Linear variable differential transformer
$m^{(V)}$	Number of fracture centers	MSJCM	Modified smooth-joint contact model
$N$	Total number of joint sets	NIOSH	National Institute for Occupational Safety and Health
$n$	Total number of data sets	PFC	Particle flow code
$\mathbf{n}$	Normal vector	PFC <sup>3D</sup>	Three-dimensional particle flow code
$n_i, n_j$	Projection of the normal vector in the directions of $i$ and $j$ , respectively	SJCM	Smooth-joint contact model
$p, p_2, p_3, q, q_2, q_3$	Empirical coefficients	UCS	Uniaxial compressive strength
$R^2$	Coefficient of determination	3DEC	Three-dimensional distinct element code
$r$	Equivalent radius		
$S_r$	Strength ratio between the jointed rock mass and intact rock strengths		
$V$	Assumed volume		
$X, Y, Z$	Cartesian coordinates		
$\lambda, \lambda_0, \lambda_2, \lambda_3$	Empirical coefficients		
$\bar{\lambda}$	Bond radius fraction of the Linear Parallel Bond Model		
$\mu$	Friction coefficient of the Linear Parallel Bond Model		
$\mu^J$	Joint friction coefficient of the Modified Smooth-Joint Contact model		
$\sigma_1, \sigma_2, \sigma_3$	Maximum, Intermediate and Minimum principal stresses, respectively		
$\sigma_c$	Uniaxial compressive strength		
$\bar{\sigma}_c, \bar{\tau}_s$	Bond tensile and shear strengths of the Linear Parallel Bond Model, respectively		
$\sigma_J, \sigma_I$	Jointed rock mass and intact rock strengths, respectively		
$\sigma_{J,i}^P$	Predicted jointed rock block strength from the new rock mass strength criterion for data set $i$		
$\sigma_{J,i}^{\text{PFC}}$	Strength of the jointed rock block from the PFC <sup>3D</sup> modeling for data set $i$		
$\bar{\sigma}_{J,i}^{\text{PFC}}$	Average strength value of all the PFC <sup>3D</sup> data		
$\sigma_n^J$	Normal stress		
$\sigma_n^J$	Normal stress on the Modified Smooth-Joint Contact		
$\varphi_J$	Joint friction angle		

## 1 Introduction

Jointed rock masses are known as the combination of intact rock blocks and discontinuities. Therefore, the mechanical behavior of a rock mass is affected by the mechanical behavior of intact rock and discontinuities in addition to the discontinuity geometry. The number of discontinuity sets, their intensity, spatial distribution of orientation, size and spacing, roughness, strength and deformation of asperities, filling, aperture, are the important properties of rock discontinuities which can affect the mechanical behavior of rock masses. Thus, assessment of the mechanical behavior of a jointed rock mass is relatively more complicated compared to that of an intact rock due to the high number of parameters that affect the mechanical behavior of rock masses (Kulatilake 1985; Yu 2001). On the other hand, unfortunately, understanding of the mechanical behavior of rock masses is crucial to design safe and economical structures in or on jointed rock masses.

Moreover, due to the presence of complicated discontinuity geometry patterns, the inherent statistical nature of discontinuity geometrical parameters, and the variabilities and uncertainties involved in the estimation of discontinuity mechanical and geometrical properties, estimation of the mechanical behavior of discontinuous rock masses is difficult and challenging (Kulatilake 1985; Kulatilake et al. 1993).

Analytical, Empirical, and numerical are three available approaches to estimate mechanical behavior of rock masses (Kulatilake et al. 1993; Singh and Goel 2011; Kulatilake 2016). Analytical approaches provide analytical solutions for rock mass strength criteria based on selecting suitable intact rock and rock joint strength criteria and applying simplified methods to combine them. This method is rarely applicable in dealing with field rock

masses, which are usually more complicated than the assumed simplified models (Bekaert and Maghous 1996; Pouya and Ghoreychi 2001).

On the other hand, the empirical approach based on one of the rock mass classification systems is simple and it may be used in complicated conditions to obtain some preliminary estimates of rock mass mechanical properties. However, in all rock mass classification systems, personal judgment, and experience play crucial roles (Bieniawski 1973; Barton et al. 1974; Hoek 1994). Moreover, in the rock mass classification systems, the isotropic behavior is assumed for the rock masses. However, most rock masses show anisotropic behavior due to the existence of distinct orientations of discontinuity sets (Kulatilake et al. 1993; Amadei 1996; Marinou et al. 2005; Wu and Kulatilake 2012; Chiu et al. 2013). Therefore, the available rock mass strength criteria based on the rock mass classification systems are unable to capture the anisotropic behavior of rock masses as well as the effect of the intermediate principal stress on the rock mass strength. It should be mentioned that even though some researchers (Pan and Hudson 1988; Priest 2005; Melkoumian et al. 2009; Zhang and Zhu 2007; Zhang 2008; Zhang et al. 2013; Saroglou and Tsiambaos 2008; Colak and Unlu 2004; Ismael et al. 2014; Yudhbir et al. 1983; Sheorey et al. 1989) tried to incorporate the effect of the intermediate principal stress in their formulations to overcome one of the above-mentioned shortcomings, their proposed criteria have not captured the effect of joint orientation and scale (resulting from joint size) on rock mass strength explicitly.

Ramamurthy (2001) instead of using the rock mass classification systems to quantify the effect of rock joint systems, proposed a joint factor parameter which is related to the joint frequency and the joint orientation. However, it does not consider the complete effect of joint orientation on rock mass strength resulting from multiple joint sets. In addition, this criterion does not consider the scale effect and the effect of the intermediate principal stress on the rock mass strength.

Nowadays through accessibility to extremely fast computers, numerical modeling can be used as an approach to overcome the shortcomings of the analytical and empirical approaches by incorporating the mechanical behavior of intact rocks and rock joints to find the mechanical behavior of rock masses (Kulatilake et al. 1993; Wu and Kulatilake 2012; Shreedharan and Kulatilake 2016). Moreover, the new methods such as digital photogrammetry and LiDAR can help to extract the geometrical properties of rock discontinuities with high resolution leading to better accuracy of numerical modeling results (Gigli and Casagli 2011; Zheng et al. 2014; Kulatilake and Shu 2015). Numerical modeling can be used to estimate rock mass strength by incorporating fracture geometry and using constitutive models for the intact rock and rock joint behavior.

For jointed rock mass strength evaluation, in addition to the above-mentioned parameters, the boundary and environmental conditions such as the in-situ stress, loading/unloading stress path, loading rate, pore pressure, temperature and humidity, are important factors to consider (Singh and Goel 2011). Thus, numerical modeling is very useful because of its power to apply different boundary conditions on the models. Polyaxial (or true-triaxial) boundary stress condition is one the most important conditions which can be considered in numerical modeling. In the polyaxial stress condition, three principal stresses (maximum principal stress,  $\sigma_1$ , intermediate principal stress,  $\sigma_2$ , minimum principal stress,  $\sigma_3$ ) are not equal ( $\sigma_1 < \sigma_2 < \sigma_3$ ) (Mehranpour and Kulatilake 2016). Although the polyaxial stress is a common condition in the real field situation which has a significant effect on the jointed rock mass strength, it has been considered rarely in the rock mechanics literature and the effect of the intermediate principal stress is generally ignored. Mehranpour and Kulatilake (2017) clearly showed the effect of the intermediate principal stress on the strength of jointed rock by extending Jaeger's theory and numerical modeling with the Particle flow code (PFC) approach, which belongs to the Discrete element method (DEM) category.

Because several parameters affect the strength of rock masses, numerous experimental tests are required to find the effect of these parameters on the strength of rock masses. That task is time consuming, very costly and impractical to perform in the field and laboratory. To solve this problem some researchers modeled rock masses with numerical modeling to propose new rock mass failure criteria. In this method, at first, a numerical model is calibrated with a limited number of experimental tests and physical modeling of the rock masses and then the calibrated model is expanded to more complicated situations with more diverse conditions (Kulatilake et al. 1993, 2001, 2006; Pouya and Ghoreychi 2001; Wu and Kulatilake 2012a; He et al. 2016). Kulatilake et al. (1993) and Wu and Kulatilake (2012) used this procedure incorporating the 3DEC software, which is one of the well-known DEM software packages used in the rock mechanics field, to find the effect of the joint geometry parameters on the deformability properties of rock masses. To quantify the joint geometry parameters, they used an extended form of the fracture tensor concept. Kulatilake et al. (2001, 2006) and He et al. (2016) also extended the fracture tensor concept to fracture tensor components and developed new rock mass strength criteria.

In this paper, the same procedure is used based on experimental tests and PFC<sup>3D</sup> modeling on intact rock, jointed rock with one joint set and jointed rock with two non-orthogonal joint sets to develop new rock mass strength criteria in three dimensions. The new criteria consider the effect of all principal stresses in three dimensions and they are applicable for any type of rock mass, especially for non-sedimentary

rock masses which generally have non-orthogonal fracture systems. This criterion also shows the anisotropic strength behavior of rock masses due to the dip angle and dip direction of joint sets. It should be mentioned that compared to other numerical methods, in the PFC, macro parameter values are not directly used in the numerical model, and micro parameter values applicable between the particles should be calibrated using the macro property values, and then these calibrated micro parameter values are used in PFC modeling.

To develop new rock mass strength criteria, first conventional experimental tests on the intact rock and the joint as well as the polyaxial compression tests on the intact rock and jointed samples are performed on the synthetic rock samples. Then the micro properties of PFC<sup>3D</sup> model are calibrated based on the experimental test results. Afterwards, polyaxial, triaxial and biaxial compression tests for the intact rock and jointed rock blocks are simulated in the PFC<sup>3D</sup> with different combinations of minimum and intermediate principal stresses. After gathering results, the development of new rock mass failure criteria was initiated using the fracture tensor concept which was introduced by Oda (1982) and developed into the fracture tensor components by Kulatilake et al. (1993, 2006). Fracture tensor combines the joint orientation, joint size, joint density for each joint set and the number of joint sets by a second order tensor. Thus, the fracture tensor can show the anisotropy and scale effects of rock masses which are exhibited by the presence of joints.

It should be mentioned that polyaxial and triaxial compression tests were performed in the laboratory with a

limited number of boundary stress conditions and joint set systems, because the experimental tests are expensive, and the apparatus had limited load capacity. Then, these experimental tests were simulated using PFC<sup>3D</sup> and the numerical results were compared with the experimental results of synthetic intact rock and synthetic jointed rock blocks. If these two groups of results did not match, micro parameter values were modified until very close results were obtained with an acceptable error. According to these steps, estimation of appropriate values for micro mechanical properties was done; it turned out to be one of the challenging parts of this project. All the above-mentioned procedures used to develop new rock mass strength criteria are shown in the flowchart given in Fig. 1.

## 2 Laboratory Tests

As mentioned in the introduction, new rock mass strength criteria were developed based on the computational results obtained from the calibrated and validated PFC<sup>3D</sup> model. Note that the macro mechanical experimental results obtained for the synthetic intact rock and synthetic rock joints were used for the calibration of the PFC<sup>3D</sup> model. Besides, a limited number of polyaxial and triaxial compression tests were also performed on the synthetic intact rock and synthetic jointed rock samples to compare with the numerical modeling results to validate the calibrated PFC<sup>3D</sup> model. In this validation procedure, it was necessary to

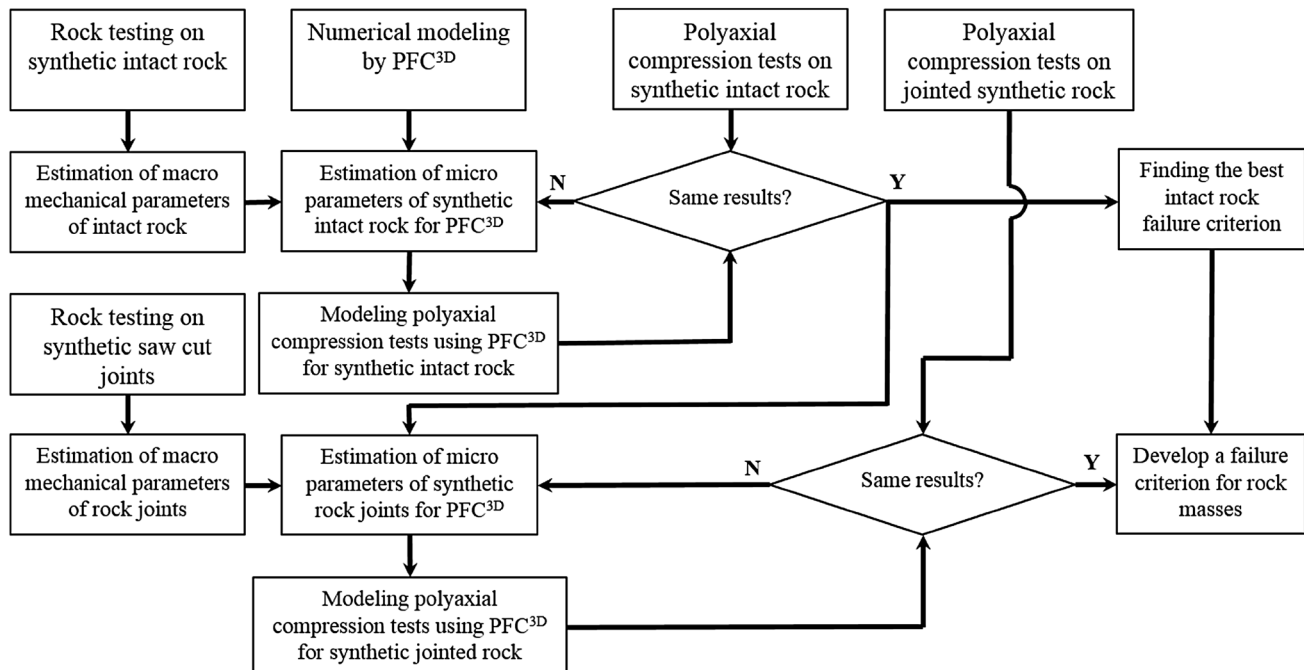


**Fig. 1** Used flowchart to develop a new rock mass failure criterion

modify the micro mechanical property values if the numerical and experimental results were not similar.

## 2.1 Sample Preparation

For the experimental part, to have several samples with the same properties, a synthetic material that was made of a mixture of gypsum, sand and water was used. This model material exhibits different mechanical properties depending on the mixture ratio. This ratio was designed to have the samples based on the loading limitation of the loading machine which was used in the laboratory. The experimental tests were performed at the China University of Mining and Technology, Beijing (CUMTB) based on the test preparation and loading conditions designed by the Rock Mass Modeling and Computational Rock Mechanics Laboratories at the University of Arizona. The water to gypsum ratio of each sample was 0.6:1 by weight. After casting the gypsum samples in the mold, samples were kept in the room temperature ( $20 \pm 2$  °C) for 1 day. Then, samples were placed in a humidity chamber which can control temperature and humidity at different levels. Samples were kept in a humidity chamber

for a week with the temperature set to  $20 \pm 2$  °C and the relative humidity set to 100%. Finally, samples were taken out from the humidity chamber and were kept in the room temperature ( $20 \pm 2$  °C) until they were used for experimental tests.

## 2.2 Intact Rock Experimental Tests

In the first step of the experimental program, three uniaxial tests, three triaxial tests and five Brazilian tests were performed on the synthetic intact rock material. Thus, from these tests, macro mechanical parameter values of the Young's modulus, uniaxial compressive strength (UCS), internal friction angle, cohesion and Poisson's ratio for the synthetic intact rock were obtained and the summary results are given in Table 1. These macro mechanical property values were used to calibrate the micro properties of the synthetic intact rock. Uniaxial and triaxial compression tests were performed on cubic samples of side dimension 160 mm. The polyaxial compression test facility available at the CUMTB (Fig. 2) was used to apply forces on all sides of the cubical samples. This machine has the capability to

**Table 1** Estimated macro mechanical property values for the synthetic rock from laboratory tests and PFC<sup>3D</sup> modeling results

	Uniaxial strength (MPa)	Tensile strength (MPa)	Cohesion (MPa)	Angle of internal friction (°)	Young's modulus (GPa)	Poisson's ratio
Experimental tests	Range 5.28–6.09	Avg. 5.78 Range 1.03–1.57	Avg. 1.23	1.9	24	Range 0.99–1.21 Avg. 1.07 0.20
PFC <sup>3D</sup> modeling	5.64	1.35	2.0	22	1.03	0.22

**Fig. 2** The polyaxial testing machine available at CUMTB

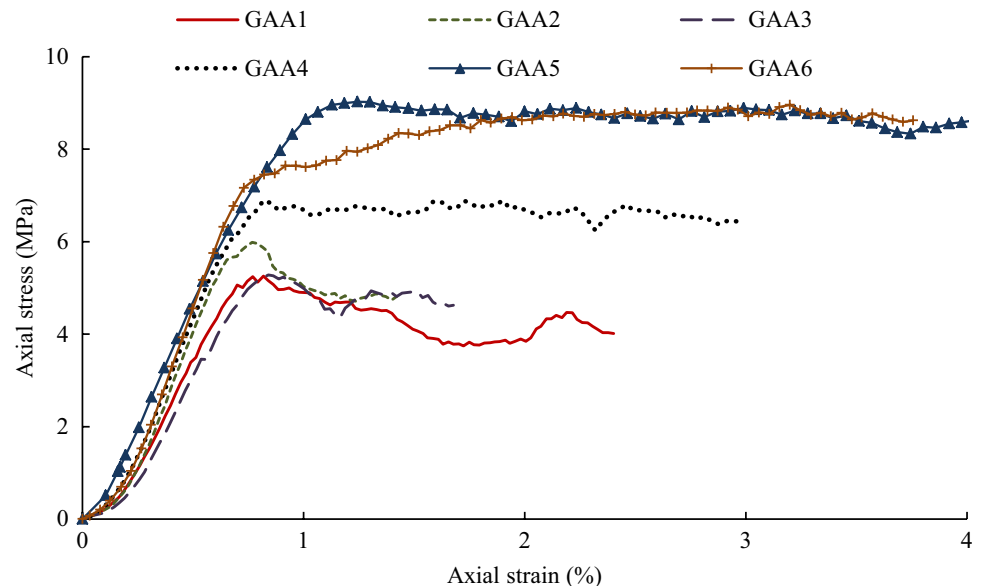


apply a maximum force of 500 KN on each of the three perpendicular directions (two horizontal directions and the vertical direction) with 0.5% accuracy. Applied load was measured in each of the perpendicular directions. Two LVDT deformation sensors were used to measure the deformation in each of the perpendicular directions. The deformation range for each direction is 150 mm with 0.4% accuracy. Loading, data collection and saving were done automatically through a data acquisition and a computer system. Figure 3 shows the uniaxial and triaxial test results obtained from the polyaxial compression test facility. These test results were used to calibrate and validate the built PFC<sup>3D</sup> model for the synthetic intact rock.

### 2.3 Rock Joint Experimental Tests

In addition to estimating the macro mechanical properties of the synthetic intact rock, it was necessary to estimate the macro mechanical properties of the synthetic rock joint to calibrate the micro mechanical properties for joints. The joint friction angle,  $\varphi_j$ , joint cohesion,  $C_j$ , joint normal stiffness,  $K_n^J$ , and the joint shear stiffness,  $K_s^J$  are important mechanical properties of the synthetic rock joint. Several researchers realized that the joint normal stiffness varies with the normal stress acting on the joint surfaces and they have proposed different relations to describe this behavior (Shehata 1972; Goodman 1976; Bandis et al. 1983; Swan 1983; Malama and Kulatilake 2003; Kulatilake et al. 2016). Kulatilake et al. (2016) developed the linear relation given by Eq. 1 between the joint normal stiffness and the normal stress acting on the joint plane,  $\sigma_n$ , and showed that it has a good correlation with experimental test results obtained by the same research group.

**Fig. 3** Uniaxial and triaxial test results; GAA1, GAA2 and GAA3 ( $\sigma_2 = \sigma_3 = 0$ ); GAA4 ( $\sigma_2 = \sigma_3 = 0.53$  MPa); GAA5 ( $\sigma_2 = \sigma_3 = 1.11$  MPa); GAA6 ( $\sigma_2 = \sigma_3 = 1.64$  MPa)



$$K_n^J = B\sigma_n \quad (1)$$

In Eq. 1,  $B$  is an empirical constant. Thus, instead of finding the joint normal stiffness the  $B$  value should be found. In this research, three direct shear tests and four joint normal stiffness tests were performed on the synthetic rock joint to estimate the macro mechanical properties of the joint and the estimated values are given in Table 2. Figure 4 shows the detailed experimental test results obtained from the direct shear tests and joint normal stiffness tests. For the direct shear tests and joint normal stiffness tests cylindrical samples with 50 mm diameter and the heights of 50 mm and 100 mm were used, respectively.

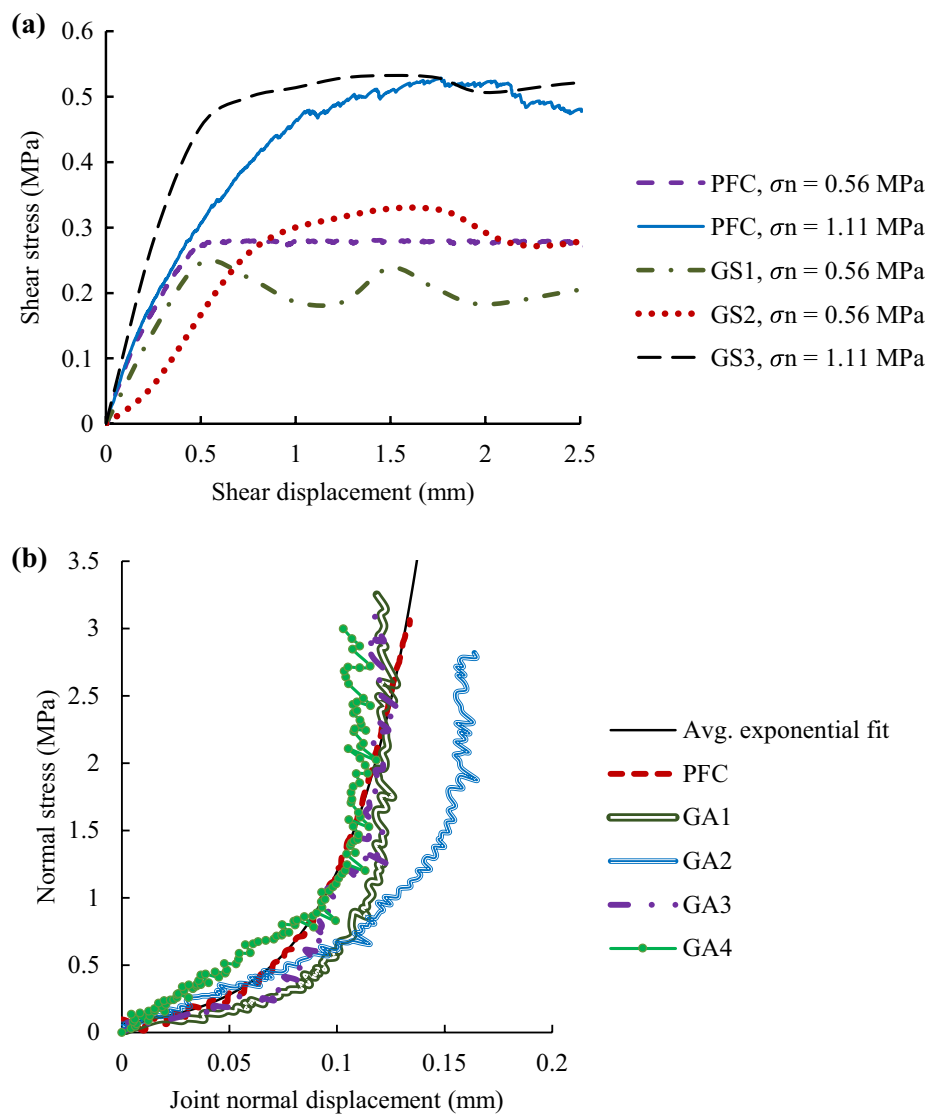
### 2.4 Polyaxial and Triaxial Compression Tests

Polyaxial and triaxial compression tests were performed on a limited number of intact rock and jointed rock samples with one joint set to verify the numerical modeling performed on the polyaxial and triaxial compression tests with the calibrated PFC<sup>3D</sup> model. The same polyaxial testing machine explained in Sect. 2.2 was used to perform the polyaxial and triaxial compression tests on the cubic synthetic intact rock

**Table 2** Estimated macro mechanical property values for the synthetic rock joint from laboratory tests and PFC<sup>3D</sup> modeling results

	Shear stiffness $B$ (1/mm) (GPa/m)		Joint friction angle (°)	
Experimental tests	Range 0.4–0.9	Avg 0.59	Range 19.8–36.8	Avg 28.9
PFC <sup>3D</sup> modeling	0.6		29	27

**Fig. 4** **a** Shear stress-shear displacement diagrams for three direct shear tests, and PFC modeling results; **b** normal stress-joint normal deformation diagrams based on four experimental jointed uniaxial compression test results, the average of the exponential fit for normal stress-joint normal deformation relation, and PFC modeling result based on the Modified Smooth Joint Contact Model



and synthetic jointed rock samples with the dimension of 160 mm. In the polyaxial test, first the minimum principal stress was applied on the sample in all three perpendicular directions. Then the stress on one lateral direction was kept constant ( $= \sigma_3$ ) and the stress equal to the intermediate principal stress was applied in the other two directions. Finally, the stress in the second lateral direction was kept constant ( $= \sigma_2$ ) and the axial stress in the vertical direction was increased until the sample failed.

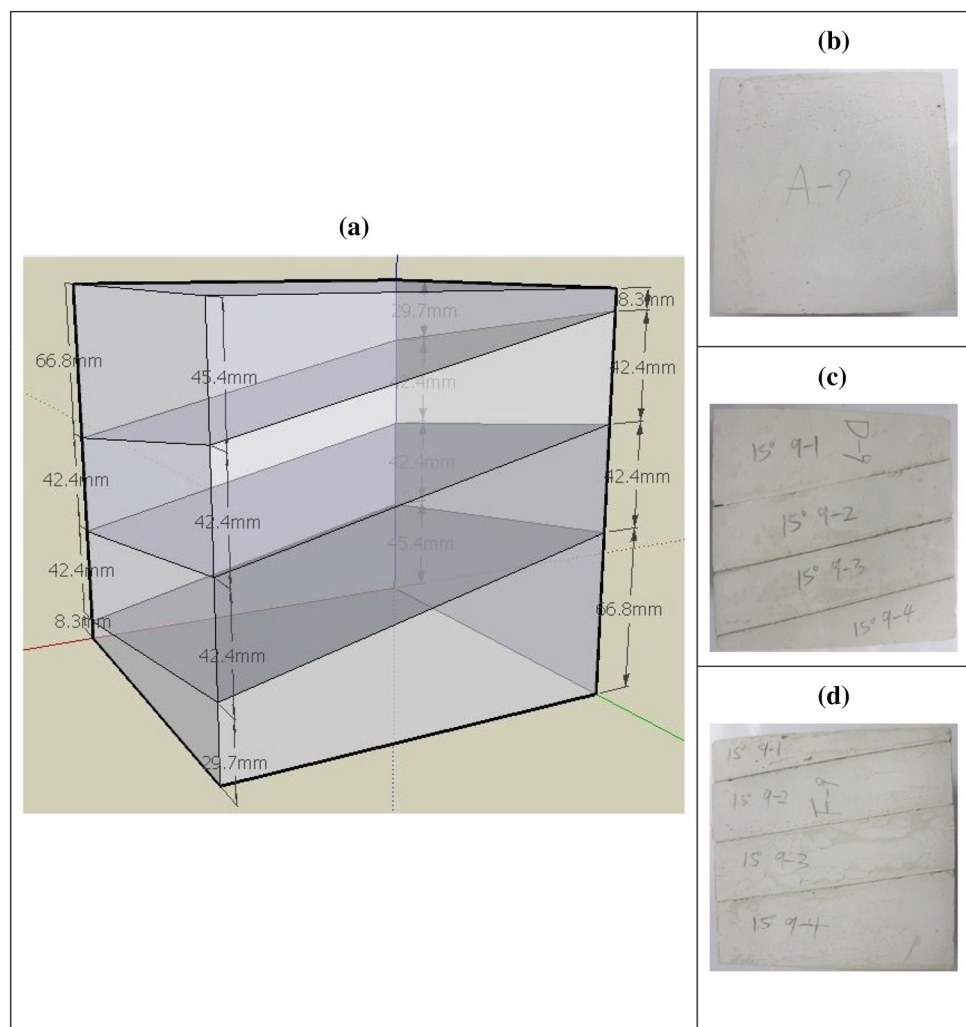
The jointed rock samples had three joints with the joint spacing of 42 mm, the dip direction of 30° and the dip angles of 15° or 30° for the different samples. Figures 5 and 6 show the schematic diagrams of these jointed samples as well as the prepared samples for experimental tests. Due to the importance of the directions of the applied principal stresses on the jointed samples for their polyaxial compression test, the same direction was used for each principal stress. For the jointed rock block samples, the maximum principal stress was applied

vertically, and the other two principal stresses were applied horizontally where the angles between the intermediate and minimum principal stress directions and the joint dip direction were 30° and 60°, respectively (Figs. 5, 6). Table 3 and Figs. 7, 8, 9 show the applied  $\sigma_2$  and  $\sigma_3$  stresses and the results of the above-mentioned experimental polyaxial and triaxial compression tests. Table 3 shows that for the same minimum principal stress, the strength of the intact rock and jointed rock increases with increasing intermediate principal stress. Besides, this table shows a strength reduction as the dip angle of the joint set increases from 15° to 30° under the same confining stresses.

### 3 Numerical Modeling

For numerical modeling, the PFC approach was chosen. The PFC is a DEM based software, which uses disks (in 2-D) or spherical elements (in 3-D) to represent particles.

**Fig. 5** Jointed rock block sample which has three joints with the dip direction of  $30^\circ$  and the dip angle of  $15^\circ$ : **a** schematic picture and the **b** top, **c** left front and **d** right front views of a prepared sample for the experimental test (the maximum principal stress applied on the top face, the intermediate principal stress applied on the left front face and the minimum principal stress applied on the right front face)



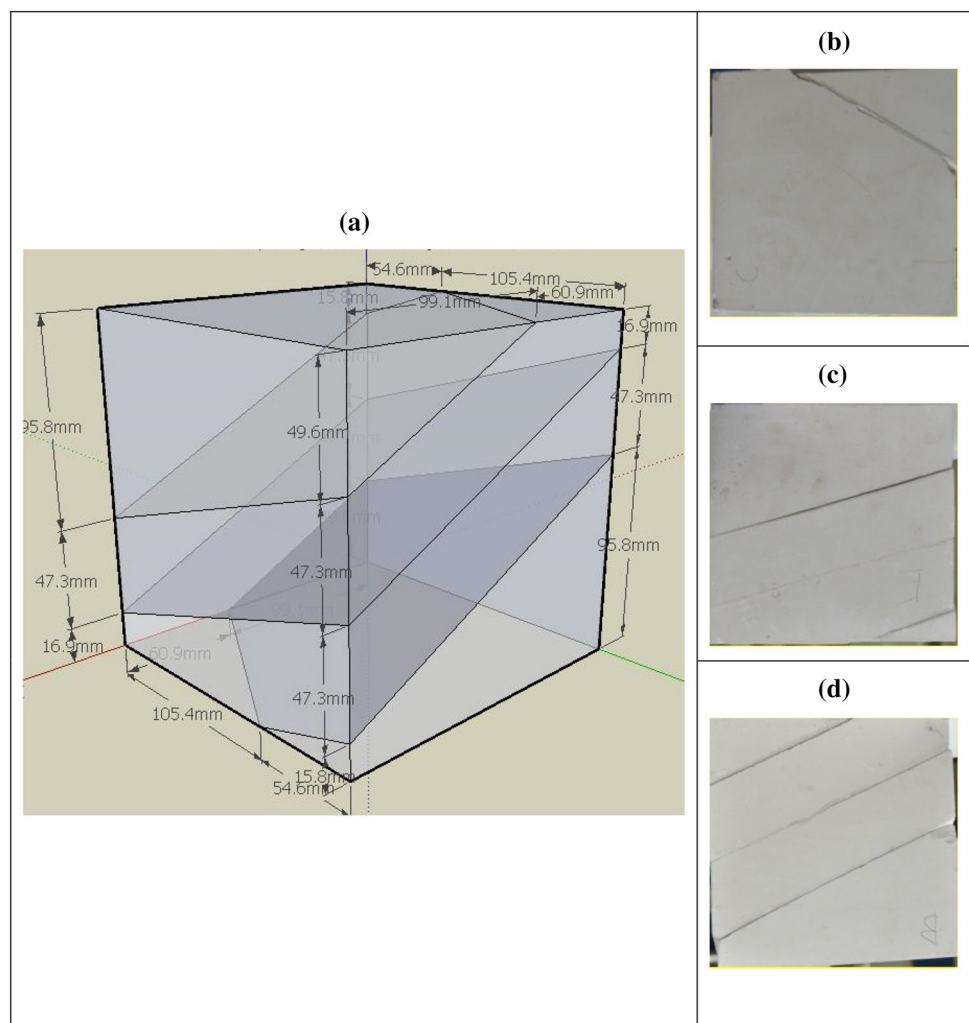
In this method, particles are assumed as rigid and Newton's second law controls the interactions between the particles. Particles can have contact with adjacent particles and force-displacement law acts at contacts (Cundall and Strack 1979; Cundall and Hart 1992). The PFC can conveniently model the fracture initiation and propagation between the particles, as well as the rupture, using the Bonded-Particle Models that cement particles together in representing the intact rock (Potyondy and Cundall 2004; Potyondy 2015). Moreover, in the PFC software to model the mechanical behavior of jointed rock masses the intact rock can be modeled by the Bonded-Particle Models, and the discontinuities can be modeled by the Smooth-Joint Contact Model (SJCM) (Pierce et al. 2007). Therefore, the block breakage as well as joint sliding can be accommodated (Mas Ivars et al. 2011).

As stated before, in the PFC, micro parameter values applicable between the particles should be calibrated using the macro properties. Due to the presence of a higher number of micro mechanical parameters compared to the available macro properties and complex behavior of the micro

mechanical parameters, the calibration of micro parameters is based on a trial and error procedure in which the micro mechanical parameter values are varied iteratively to match the macro mechanical behaviors. Therefore, the calibration is one of the most critical and challenging parts in modeling with the PFC. Several researchers such as Kulatilake et al. (2001), Potyondy and Cundall (2004), Cho et al. (2007), Yang et al. (2015) and Mehranpour and Kulatilake (2016) have dealt with this calibration and have indicated their findings on relations between the micro and macro parameters. Several others have used the PFC in modeling intact rocks or jointed rock masses (Fakhimi 2004; Koyama and Jing 2007; Park and Song 2009; Lee and Jeon 2011; Schöpfer et al. 2013; Zhang et al. 2015; Fan et al. 2015; Duan and Kwok 2016). However, limited efforts (Yang et al. 2015; Bahaaddini et al. 2015; Mehranpour and Kulatilake 2017) have been made on the calibration and modeling of the joints with the SJCM.

In this research to model the intact rock in PFC<sup>3D</sup>, among the different bonded particle models, the linear parallel bond

**Fig. 6** Jointed rock block sample which has three joints with the dip direction of  $30^\circ$  and the dip angle of  $30^\circ$ : **a** schematic picture and the **b** top, **c** left front and **d** right front views of a prepared sample for the experimental test (the maximum principal stress applied on the top face, the intermediate principal stress applied on the left front face and the minimum principal stress applied on the right front face)



model (LPBM) was chosen for contacts. The LPBM works like a cement material and assumes the two adjacent particles are cemented to each other with a notional rectangular (2D) or cylindrical (3D) shape of contact. The major problem of LPBM is its inability to model the failure envelop for the whole spectrum of rock types. It can only model rocks with the low internal friction angles, and the low ratios of compressive to tensile strength. To solve this problem some researchers have proposed different methods and different models (Potyondy and Cundall 2004; Fakhimi 2004; Cho et al. 2007). The synthetic material which is used in this study has a low internal friction angle and a low ratio of compressive to tensile strength. Thus, the LPBM can model the used synthetic intact rock properly.

For the synthetic intact rock calibration process a cubic sample of side dimension of 160 mm with a uniform particle size distribution (the minimum particle diameter of 2.7 mm and the maximum particle diameter of 4.48 mm) was created in PFC<sup>3D</sup> to model the uniaxial and triaxial tests mentioned in Sect. 2.2. Based on the selected particle

size distribution, 103,663 particles and 275,824 contacts were produced in the cubic samples of side dimension of 160 mm. For the Linear Parallel Bond Model used for the synthetic intact rock, it is necessary to calibrate the micro mechanical parameters of contact Young's modulus,  $E_c$ , bond Young's modulus,  $\bar{E}_c$ , contact friction coefficient,  $\mu$ , bond tensile strength,  $\bar{\sigma}_c$ , bond shear strength,  $\bar{\tau}_s$ , the ratio of normal to shear stiffness for contact,  $k_r$ , ratio of normal to shear stiffness for bond,  $\bar{k}_r$ , and bond radius fraction,  $\bar{\lambda}$ , using macro properties of the uniaxial compressive strength, internal friction angle, Young's modulus, tensile strength and Poisson's ratio. Because the number of micro mechanical parameters is higher than the number of macro mechanical parameters, the assumptions of  $E_c = \bar{E}_c$ ,  $k_r = \bar{k}_r$ ,  $\bar{\sigma}_c = \bar{\tau}_s$  and  $\bar{\lambda} = 1$  were used as recommended by Potyondy and Cundall (2004) and Itasca (2016) to reduce the calibration process difficulty. As stated before, the calibration is a trial and error procedure. Therefore, to minimize the number of iterations in the calibration process the following sequence was followed based on the

**Table 3** Experimental and PFC<sup>3D</sup> modeling results of the polyaxial and triaxial compression tests for the synthetic intact rock and the jointed rock blocks having three joints with the dip direction of 30° and joint dip angles of 15° or 30°

	Sample	$\sigma_3$ (MPa)	$\sigma_2$ (MPa)	$\sigma_1$ (MPa) Experimental	$\sigma_1$ (MPa) PFC <sup>3D</sup>
Intact rock	GB1	0	1.128	6.030	6.431
	GB2	0	2.256	6.642	6.763
Jointed rock (dip direction = 30°)					
Dip = 15°	GC15-1	1.128	3.384	8.301	8.325
	GC15-2	1.128	4.512	9.075	8.475
	GC15-3	2.256	2.256	9.165	9.200
	GC15-4	2.256	4.512	10.792	10.761
	GC15-5	2.256	7.896	10.856	11.151
	GC15-6	3.384	3.384	11.266	11.447
Dip = 30°	GC30-1	1.128	5.640	8.124	7.595
	GC30-2	2.256	2.256	8.304	7.742
	GC30-3	2.256	5.640	9.311	9.723
	GC30-4	2.256	7.896	9.578	9.779
	GC30-5	3.384	3.384	9.460	9.751

relations between micro and macro mechanical properties and the guidelines given by Yang et al. (2015) and Mehranpour and Kulatilake (2016). First, in the uniaxial compression test modeling the Young's modulus was calibrated by setting the material strengths to a large value and varying  $E_c$  and  $\bar{E}_c$  to match the Young's modulus. Next, by changing  $k_r$  and  $\bar{k}_r$ , the Poisson's ratio was matched. After calibrating the above-mentioned micro mechanical parameters, the peak strength was matched by gradually reducing the normal and shear bond strengths of the parallel bonds. Finally, by gradual reduction of  $\mu$  in modeling of the triaxial compression tests, the internal friction angle was matched. The calibrated micro parameter values are given in Table 4 for Linear Parallel Bond Model. Table 1 shows the obtained macro mechanical parameter values based on PFC<sup>3D</sup> simulations as well as from laboratory

tests. Comparison of the two sets of values indicates the accuracy and capability of the particle flow approach in simulating the synthetic intact rock.

To model the synthetic rock joint in PFC<sup>3D</sup>, the Modified Smooth-Joint Contact model (MSJCM) was used. The MSJCM was proposed by Mehranpour and Kulatilake (2017) to overcome the shortcoming of the Smooth Joint Contact Model (SJCM) to capture the non-linear behavior of the joint closure varying with the joint normal stress. The MSJCM uses the linear relation between the joint normal stiffness and the normal contact stress given in Eq. 1 to model the non-linear relation between the joint normal deformation and the joint normal stress observed in the compression joint normal stiffness test. Thus, in the MSJCM instead of assigning a constant value to the joint normal stiffness,  $k_n^J$ , a variable value is assigned which is proportional to the normal stress on the smooth-joint contact,  $\sigma_n^J$ , according to the following equation.

$$k_n^J = \max\left(k_{n_{\min}}^J, B^J \sigma_n^J\right). \quad (2)$$

In Eq. 2,  $k_{n_{\min}}^J$  is the minimum value for  $k_n^J$ , and  $B^J$  is a constant coefficient. It should be mentioned that  $k_{n_{\min}}^J$  is included since it is impossible to have a zero value for stiffness in PFC. Note that the other micro mechanical parameters for the MSJCM like joint shear stiffness,  $k_s^J$ , and joint friction coefficient,  $J$ , are the same as for the SJCM.

Mehranpour and Kulatilake (2017) also proposed a new joint contact implementation algorithm in PFC which is called the joint sides checking (JSC) approach to solve the interlocking problem. The interlocking problem was observed by Bahaaddini et al. (2013) and it occurs due to the shortcoming of the updating procedure in the PFC software for the contact conditions of the particles that lie around the intended joint plane during high shear displacements. The interlocking problem leads to higher values for shear strength and dilation angle for the joint than the correct values. It also creates unwanted fractures around the intended

**Fig. 7** Experimental and PFC<sup>3D</sup> modeling results of the polyaxial compression test for the intact rock subjected to **a**  $\sigma_3=0$  and  $\sigma_2=1.128$  MPa, **b**  $\sigma_3=0$  MPa and  $\sigma_2=2.256$  MPa

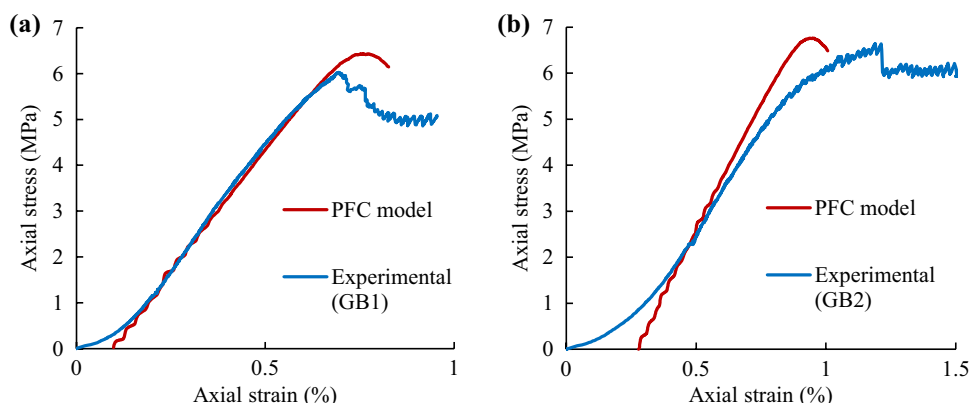
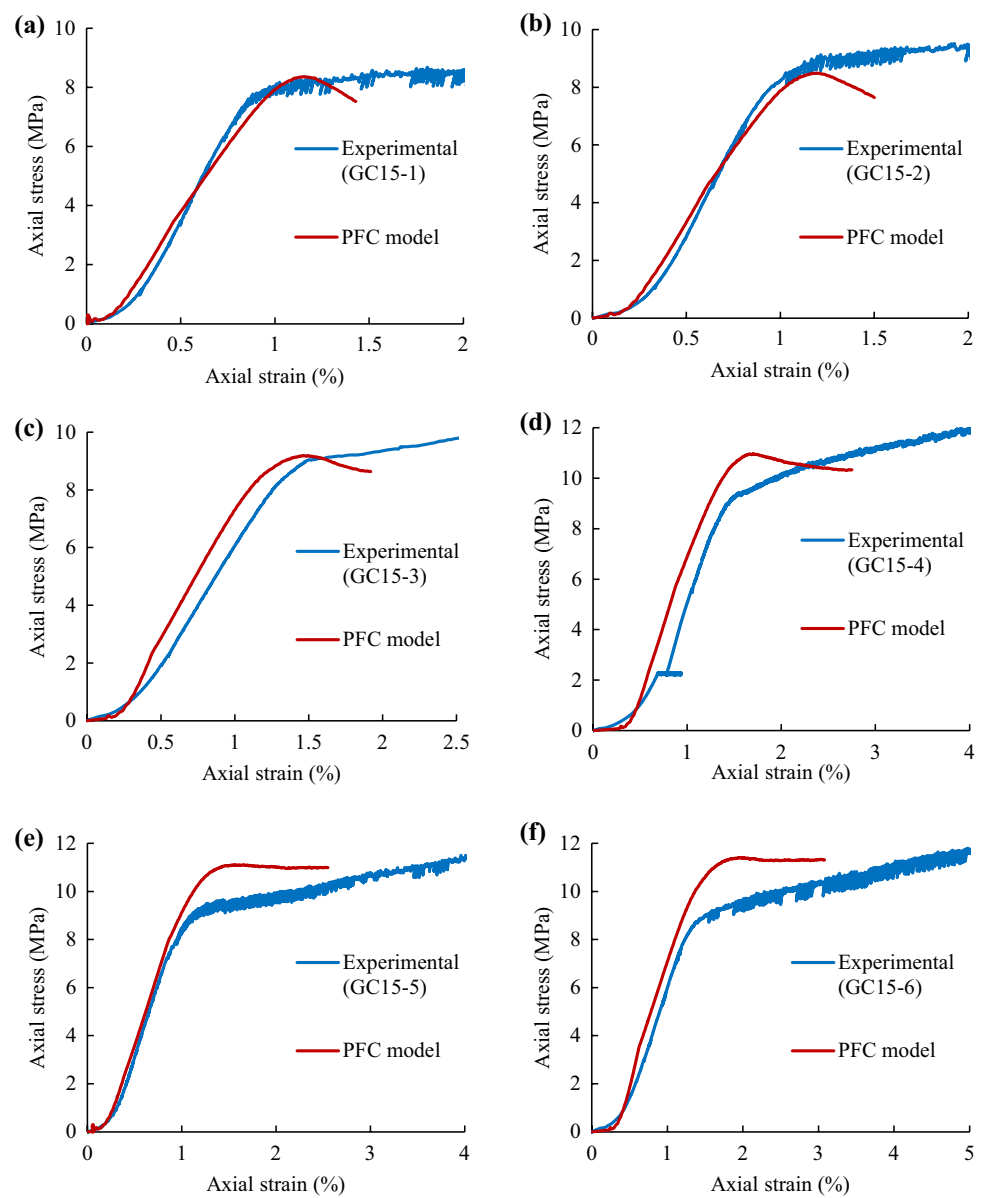


**Fig. 8** Experimental and PFC<sup>3D</sup> modeling results of the polyaxial and triaxial compression tests for the jointed rock block samples having one joint set with the joint dip direction of 30° and dip angle of 15° subjected to a  $\sigma_3 = 1.128$  MPa and  $\sigma_2 = 3.384$  MPa, b  $\sigma_3 = 1.128$  MPa and  $\sigma_2 = 4.512$  MPa, c  $\sigma_3 = \sigma_2 = 2.256$  MPa, d  $\sigma_3 = 2.256$  MPa and  $\sigma_2 = 4.512$  MPa, e  $\sigma_3 = 2.256$  MPa and  $\sigma_2 = 7.896$  MPa and f  $\sigma_3 = \sigma_2 = 3.384$  MPa



joint plane. In this paper, the JSC approach is used not only for the calibration procedure of the rock joint model but also for the modeling of the polyaxial, triaxial and biaxial compression tests on the synthetic jointed rock block samples.

In calibrating the joint micro mechanical parameters, first the cylindrical synthetic rock samples with 50 mm diameter, and the heights of 50 and 100 mm were numerically modeled based on the linear parallel bond model properties given in Table 4, for the direct shear tests and the joint normal stiffness test, respectively. Then the MSJCM joint was added horizontally to each sample at the mid-height level with the JSC approach. Then, to calibrate the MSJCM the following sequence was used to minimize the number of iterations. First, all the micro mechanical parameters for MSJCM were set with low values. Then,

$k_{n_{\min}}^J$  and  $B^J$  were calibrated using the joint normal stiffness test modeling because  $k_s^J$  and  $J$  values do not affect this test results. In the calibration of joint normal stiffness test, first the  $B^J$  value was gradually increased to match the curvature of the normal stress-joint normal displacement diagram and then by increasing the  $k_{n_{\min}}^J$ , the total joint normal displacement was matched (see Fig. 4a). After  $k_{n_{\min}}^J$  and  $B^J$  calibration, in the direct shear test modeling, first  $k_s^J$  was gradually increased to match  $K_s^J$  and finally, the  $J$  value was changed to match the  $\varphi_J$  value (see Fig. 4b). Table 5 shows the calibrated micro mechanical property values of the MSJCM using the JSC approach based on the experimental test results reported for the synthetic rock joint in

**Fig. 9** Experimental and PFC<sup>3D</sup> modeling results of the polyaxial and triaxial compression tests for the jointed rock samples having one joint set with the joint dip direction of 30° and dip angle of 30° subjected to **a**  $\sigma_3 = 1.128$  MPa and  $\sigma_2 = 5.640$  MPa, **b**  $\sigma_3 = \sigma_2 = 2.256$  MPa, **c**  $\sigma_3 = 2.256$  MPa and  $\sigma_2 = 5.640$  MPa, **d**  $\sigma_3 = 2.256$  MPa and  $\sigma_2 = 7.896$  MPa and **e**  $\sigma_3 = \sigma_2 = 3.384$  MPa

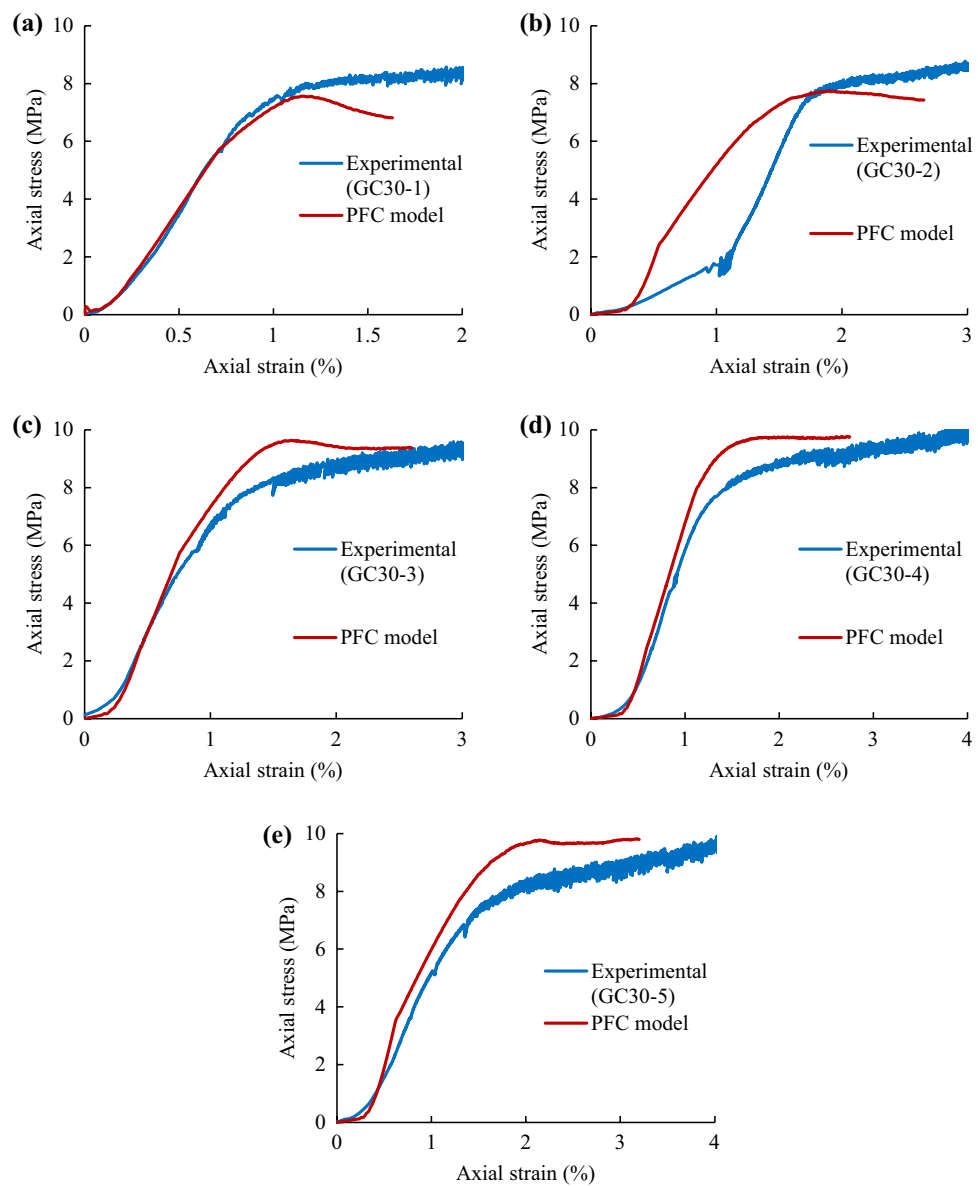


**Table 4** Calibrated micro mechanical parameter values of the linear parallel bond model for the synthetic intact rock in PFC<sup>3D</sup> (minimum particle diameter,  $D_{\min}$ , maximum particle diameter,  $D_{\max}$ , contact Young's modulus,  $E_c$ , bond Young's modulus,  $\bar{E}_c$ , contact friction coefficient,  $\mu$ , bond tensile strength,  $\bar{\sigma}_c$ , bond shear strength,  $\bar{\tau}_s$ , the ratio of normal to shear stiffness for contact,  $k_r$ , ratio of normal to shear stiffness for bond,  $\bar{k}_r$  and bond radius fraction,  $\lambda$ )

#### LPBM

$D_{\min} = 27$  mm  
 $m_r = D_{\max}/D_{\min} = 1.66$   
 $E_c = \bar{E} = 1.25$  GPa  
 $k_r = \bar{k}_r = 2.5$   
 $\mu = 0.6$   
mean  $\bar{\sigma}_c$  = mean  $\bar{\tau}_s = 4.4$  MPa  
std. dev.  $\bar{\sigma}_c$  = std. dev.  $\bar{\tau}_s = 1.1$  MPa  
 $\bar{\lambda} = 1$

**Table 5** Calibrated micro mechanical parameter values of the Modified Smooth Joint Contact Model for the synthetic rock joint in PFC<sup>3D</sup> using the JSC approach

MSJCM
$\mu^J = 0.5$
$k_s^J (GPa/m) = 1.0$
$k_{n_{\min}}^J (GPa/m) = 4.0$
$B^J (1/mm) = 31.0$

Sect. 2.3. Table 2 shows the obtained macro mechanical parameter values based on the PFC<sup>3D</sup> simulations. Note that Table 2 also provides the macro mechanical parameter values obtained through experimental joint testing. Table 2 along with Fig. 4 indicate the accuracy and capability of the PFC in simulating the synthetic rock joint through comparison of PFC<sup>3D</sup> results against the laboratory test results on synthetic rock joints. For further details about

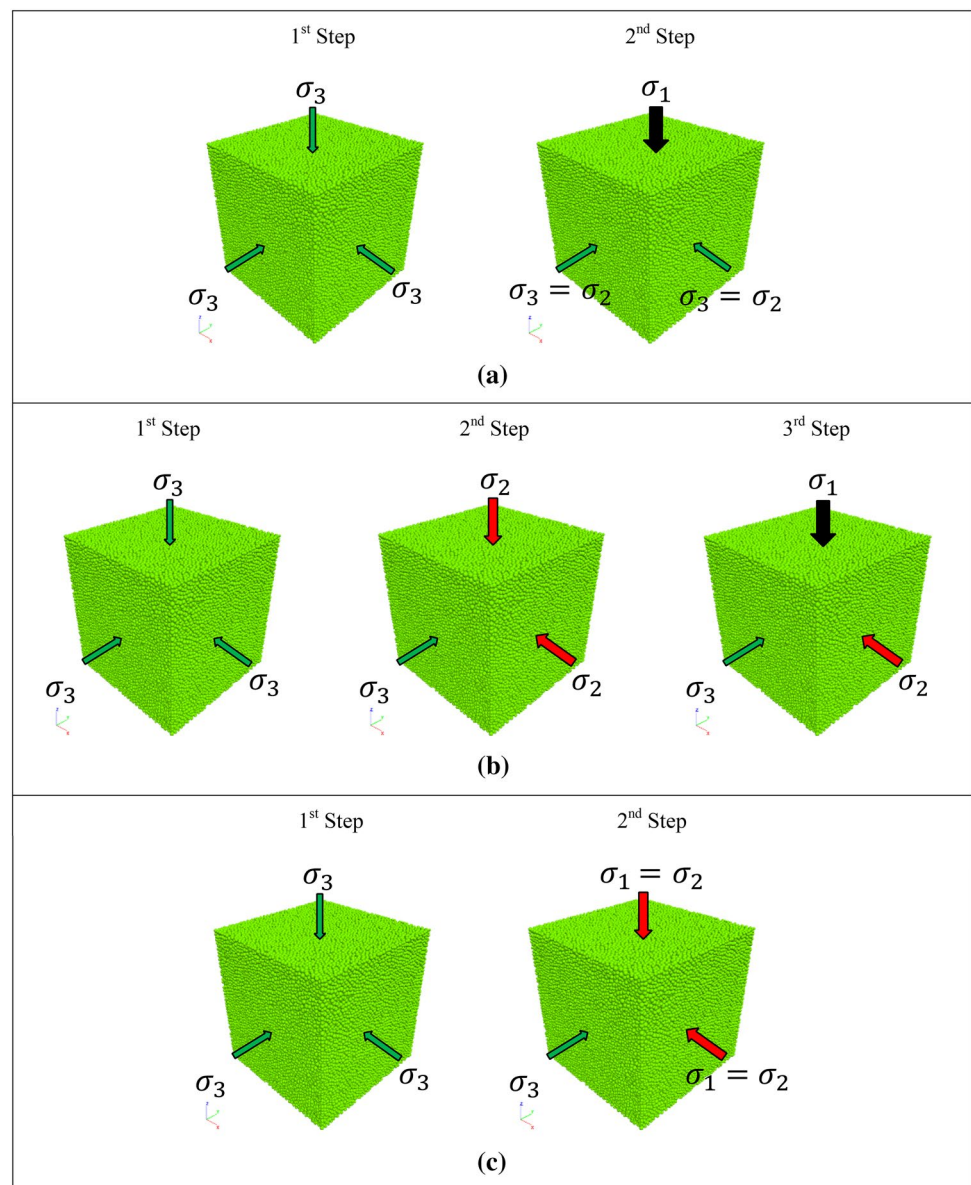
the JSC approach, MSJCM and the interlocking problem the reader is referred to Mehranpour and Kulatilake (2017).

### 3.1 Polyaxial Compression Tests

In the performed numerical modeling, three different test types were simulated on the synthetic intact rock and synthetic jointed rock blocks using PFC<sup>3D</sup> to obtain data to develop suitable rock mass strength criteria. In these simulations like the experimental tests, cubic samples of side dimension 160 mm were used with micro mechanical property values given in Tables 4 and 5. The first test type conducted was the triaxial test ( $\sigma_1 > \sigma_2 = \sigma_3$ ). In simulating this test, the hydraulic stress equal to the minimum principal

stress was applied on the sample until the sample reached the equilibrium (1st step in Fig. 10a). Then the stresses on the lateral faces were kept constant ( $= \sigma_2 = \sigma_3$ ) and the axial stress was increased until the sample failed (2nd step in Fig. 10a). The second type of test simulated was the polyaxial (true-triaxial) test ( $\sigma_1 > \sigma_2 > \sigma_3$ ). In this test like in the conventional triaxial test, the hydraulic stress equal to the minimum principal stress was applied on the sample until the sample reached the equilibrium (1st step in Fig. 10b). Then the stress on one lateral direction was kept constant ( $= \sigma_3$ ) and the stress equal to the intermediate principal stress was applied in the other two directions until the sample reached the equilibrium (2nd step in Fig. 10b). Finally, the stress in the second lateral direction was kept constant ( $= \sigma_2$ ) and the axial stress in the vertical direction was

**Fig. 10** Different steps of applying the minor, intermediate and major principal stresses for the **a** triaxial compression tests, **b** polyaxial compression tests and **c** biaxial compression tests



increased until the sample failed (3rd step in Fig. 10b). The third test type simulated was the biaxial test ( $\sigma_1 = \sigma_2 > \sigma_3$ ). In this test like in the two previous tests, the hydraulic stress equal to the minimum principal stress was applied on the sample until the sample reached the equilibrium (1st step in Fig. 10c). Then the stress on one lateral direction was kept constant ( $= \sigma_3$ ) and the stresses in the other two directions were increased until the sample failed (2nd step in Fig. 10c).

The minimum and intermediate principal stress combination values of different compression tests were chosen based on the UCS value of the modeled synthetic intact rock. The minimum principal stress values were chosen as 0, 20, 40 and 60% of the UCS. For each minimum principal stress value, the intermediate principal stress value varied starting at the minimum principal stress value and increasing at an interval of 20% of the UCS until it was slightly lower than the strength of the sample under the biaxial loading condition with the same minimum principal stress value. With this procedure, the applied minimum and intermediate principal stress combinations for samples were the same. Thus, the effect of joint geometry configurations on the rock mass strength can be evaluated properly. Moreover, because the strength of the synthetic intact rock is available for each minimum and intermediate principal stress combination, the normalized strength of jointed rock blocks can be obtained to propose a general rock mass strength criterion.

For jointed rock blocks, twelve different joint systems with one and two joint sets were chosen to cover different types of non-orthogonal fracture systems. Joint sets have different dip angles varying from  $15^\circ$  to  $45^\circ$  at an interval of  $15^\circ$  with dip directions of  $30^\circ$  and  $75^\circ$ . Each joint set has 3 joints with the joint spacing of 42 mm in a cubic sample of size 160 mm. Figure 11 shows the PFC<sup>3D</sup> models and the schematic pictures of joint geometry diagrams for all 12 jointed rock blocks. It should be mentioned that for each cubic sample, the minimum principal stress was applied on the faces with the dip directions of  $90^\circ$  and  $270^\circ$  and the intermediate principal stress was applied on the faces with the dip directions of  $0^\circ$  and  $180^\circ$ . It should be mentioned that because the numerical models based on the micro parameter values given in Tables 4 and 5 could reasonably accurately model the experimental test results up to the sample failure (Figs. 7, 8, 9), it was not necessary to modify the micro parameter values given in Tables 4 and 5. For each rock joint system under each confining stress combination it took about 2 days on the average to complete an above-mentioned numerical simulation. However, this time duration was smaller for models with lower confining stresses and joint systems with lower dip angles compared to that having higher confining stresses and higher dip angles.

Figures 12, 13, 14 and 15 show the rock block strength values obtained for the synthetic jointed and intact rock models under different minimum and intermediate principal

stress combinations. Figure 12 shows the rock strength values obtained for the synthetic jointed rock models with one joint set compared to the strength of the synthetic intact rock model and Figs. 13, 14 and 15 show the rock strength values obtained for the synthetic jointed rock models with two joint sets under different minimum and intermediate principal stress combinations compared to the strength of the synthetic jointed rock models having one joint set with the same properties as the first joint set of the rock sample with two joint sets. These figures indicate that for each combination of the minimum and intermediate principal stresses, the jointed rock blocks with two joint sets and first joint set have resulted in a lower strength compared to that of the synthetic intact rock and the jointed rock blocks with two joint sets have resulted in a lower strength value compared to that of the jointed rock blocks having one joint set with the same properties as the first joint set of the rock sample with two joint sets. This means that adding of joint sets to a sample under the same minimum and intermediate principal stress combination reduces the strength of the sample.

Figure 12 also shows that the intermediate principal stress has a significant effect on the synthetic intact rock strength and it can increase the intact rock strength up to about 25%. Increase of the intermediate principal stress while keeping the minimum principal stress constant, increases the strength of intact rock to a peak value and then the strength decreases. However, in Fig. 12, 13, 14, 15 for each  $\sigma_3$  level in the jointed rock models, the reduction of the strength after reaching the peak strength due to increase of  $\sigma_2$  seems to be lower compared to that of the intact rock model. In some plots, even the strength reduction does not seem to exist especially for low  $\sigma_3$  values and high joint set dip angles.

## 4 Development of New Rock Mass Strength Criteria

This paper develops new rock mass strength criteria based on the PFC<sup>3D</sup> modeling results incorporating the fracture tensor concept. The fracture tensor is explained comprehensively in references (Oda 1982, 1984; Kulatilake et al. 1993; Wu and Kulatilake 2012). In the fracture tensor, it is assumed that each fracture to be a very thin disk having an area  $A$  with an equivalent radius of  $r$  ( $A = \pi r^2$ ) and two normal vectors of  $\mathbf{n}$  and  $-\mathbf{n}$  (bold italic letter represent a vector) for each side of the disk. To find the fracture tensor components of the modeled jointed rock blocks the following equations are used.

$$F_{ij}^r = \sum_{k=1}^N F_{ij}^k \quad (3)$$

**Fig. 11** The jointed rock blocks modeled by the PFC<sup>3D</sup> and the schematic pictures of joint systems: **a**, **b** and **c** have three joints with the dip direction of  $30^\circ$  and the dip angles of  $15^\circ$ ,  $30^\circ$  and  $45^\circ$ , respectively; **d**, **e** and **f** have six joints formed from two joint sets,  $30^\circ$  joint dip direction and  $15^\circ$  joint dip angle for the first joint set and  $75^\circ$  joint dip direction and the dip angles of  $15^\circ$ ,  $30^\circ$  and  $45^\circ$  for the second joint set, respectively; **g**, **h** and **i** have six joints formed from 2 joint sets,  $30^\circ$  joint dip direction and  $30^\circ$  joint dip angle for the first joint set and  $75^\circ$  joint dip direction and the dip angles of  $15^\circ$ ,  $30^\circ$  and  $45^\circ$  for the second joint set, respectively; **j**, **k** and **l** have six joints formed from two joint sets,  $30^\circ$  joint dip direction and  $45^\circ$  joint dip angle for the first joint set and  $75^\circ$  joint dip direction and the dip angles of  $15^\circ$ ,  $30^\circ$  and  $45^\circ$  for the second joint set, respectively; (in the schematic pictures, the blue planes are 1st joint set and red planes are 2nd joint set; the maximum principal stress, the intermediate principal stress and the minimum principal stresses are applied on the top face, on the front left face and on the right front face, respectively)

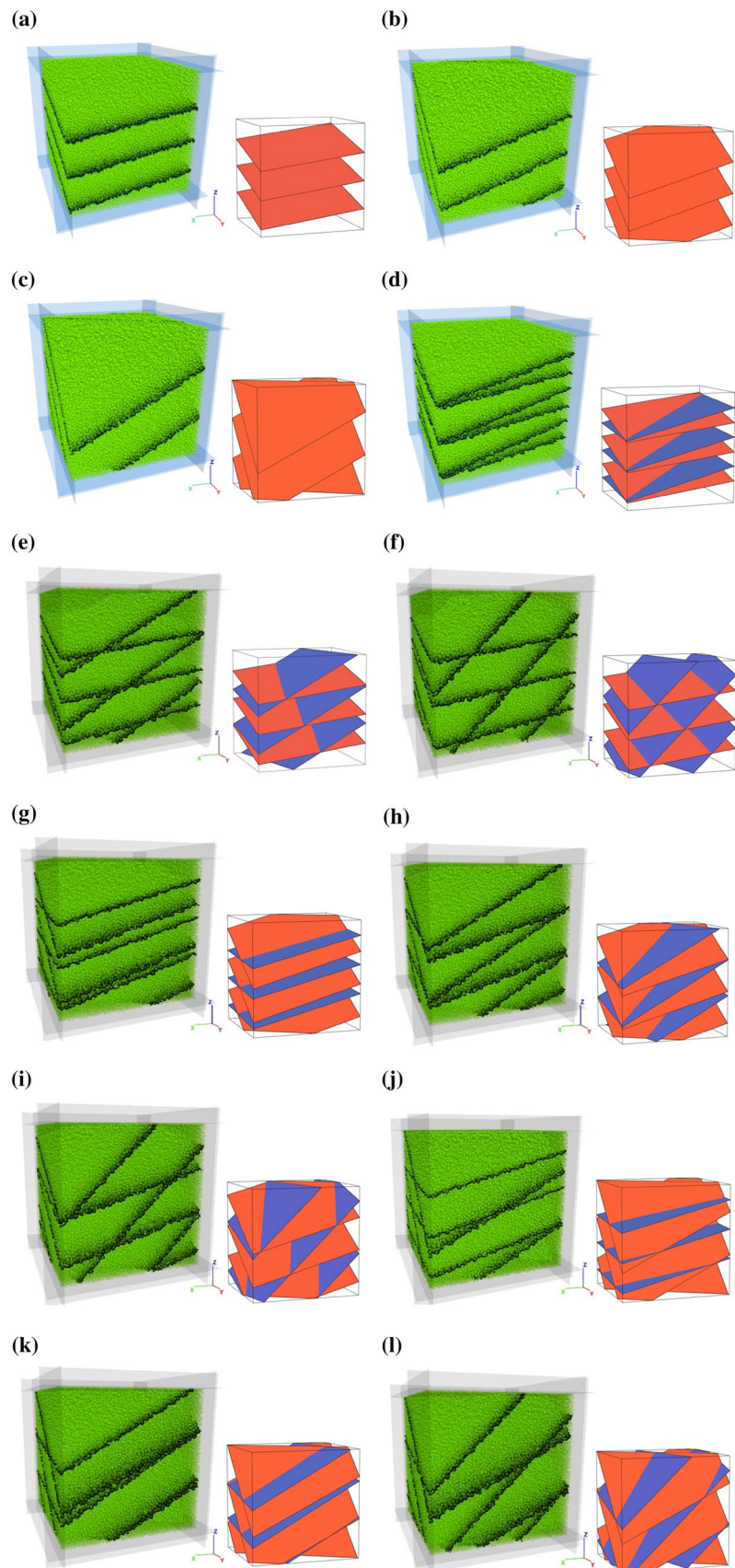


**Fig. 12** Polyaxial test results obtained from PFC<sup>3D</sup> modeling for the intact rock model and jointed rock models with one joint set having three joints with the dip direction of 30° and the various joint dip angles from 15° to 45° at an interval of 15°

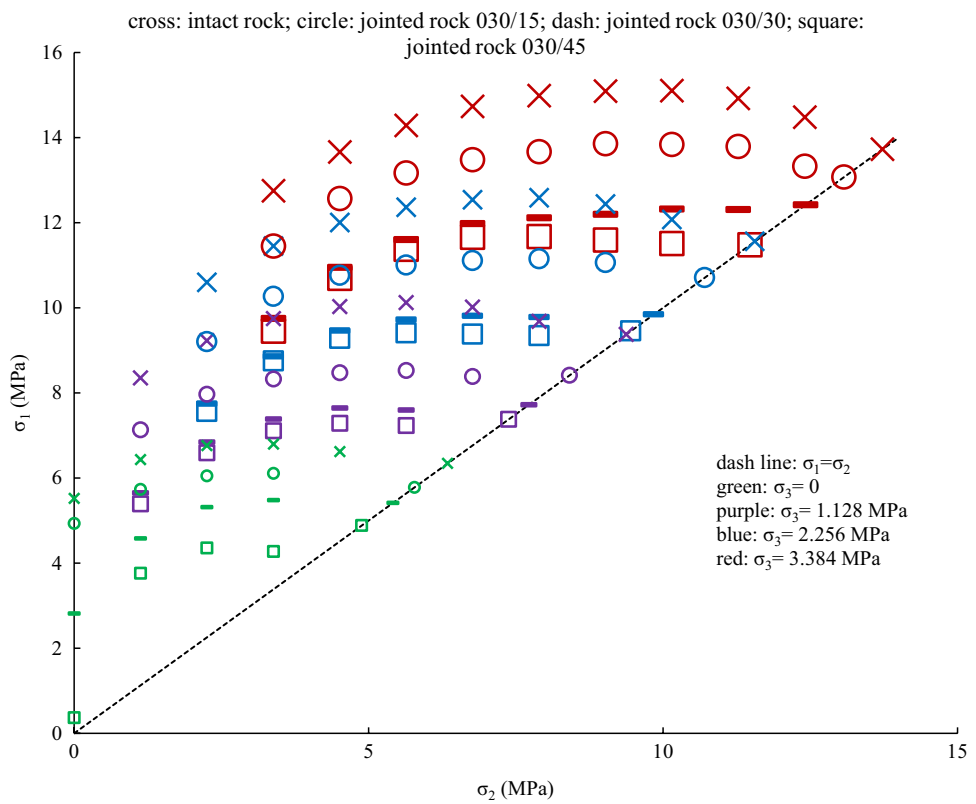


**Fig. 13** Polyaxial test results obtained from PFC<sup>3D</sup> modeling for the jointed rock model having 3 joints with 30° joint dip direction and 15° joint dip angle and the jointed rock models having six joints formed from two joint sets with 30° joint dip direction and 15° joint dip angle for the first joint set and 75° joint dip direction and the various joint dip angles from 15° to 45° at an interval of 15° for the second joint set

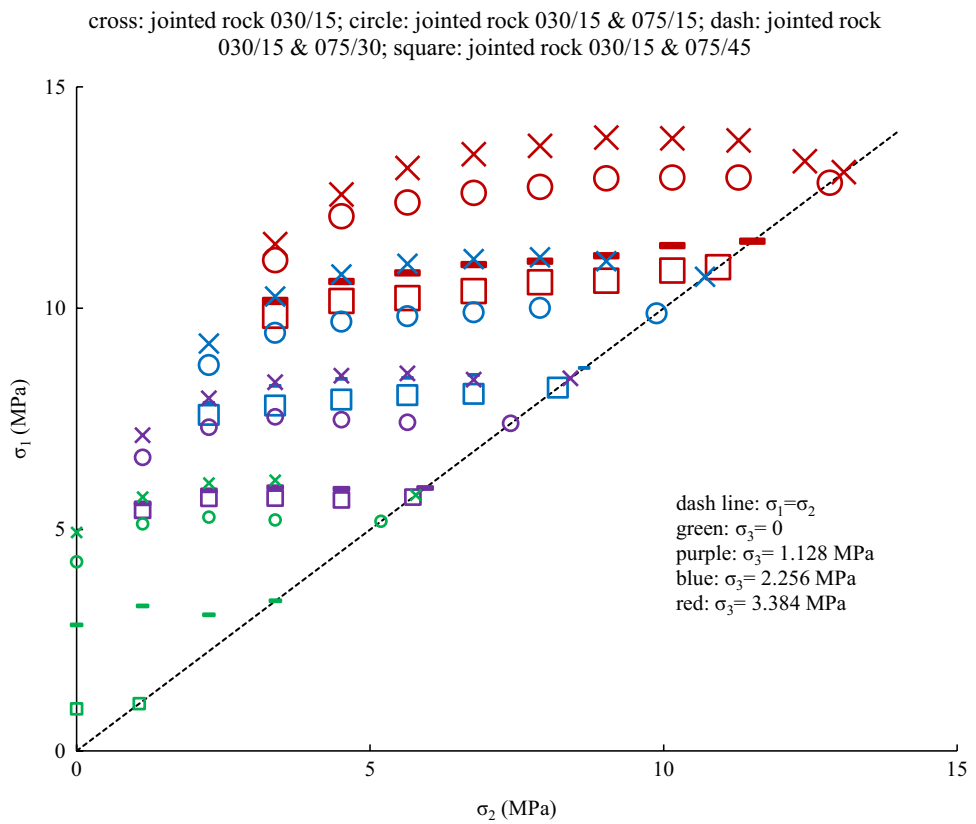


**Fig. 14** Polyaxial test results obtained from PFC<sup>3D</sup> modeling for the jointed rock model having three joints with 30° joint dip direction and 30° joint dip angle and the jointed rock models having six joints formed from two joint sets with 30° joint dip direction and 30° joint dip angle for the first joint set and 75° joint dip direction and the various joint dip angles from 15° to 45° at an interval of 15° for the second joint set

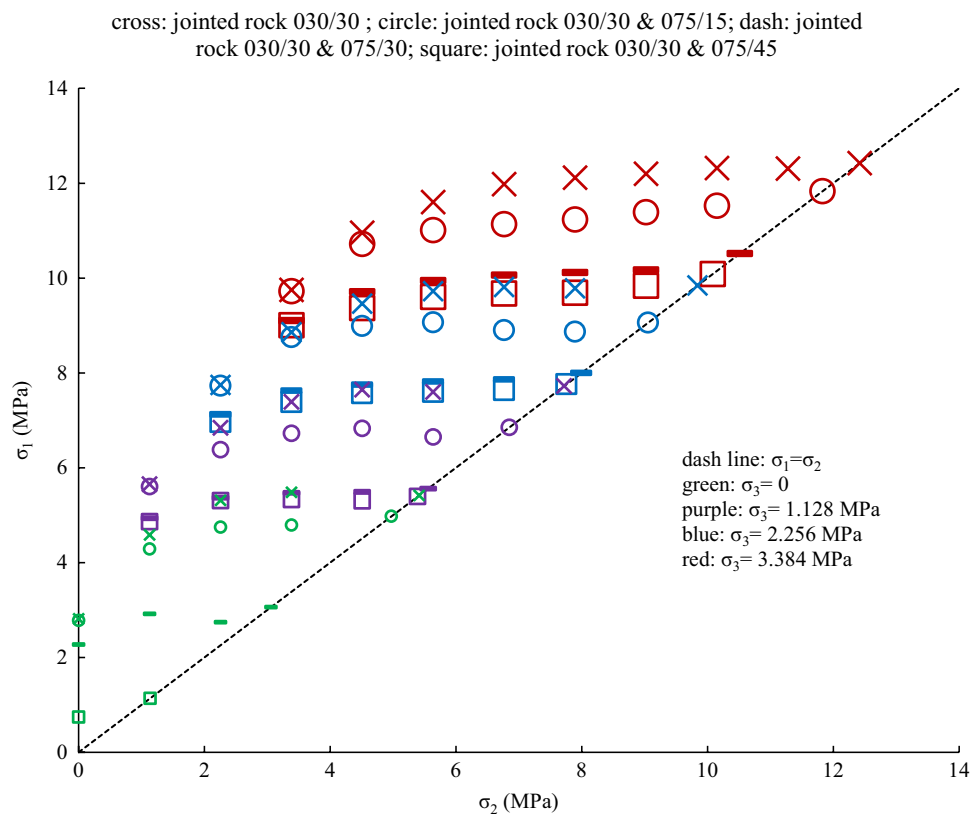
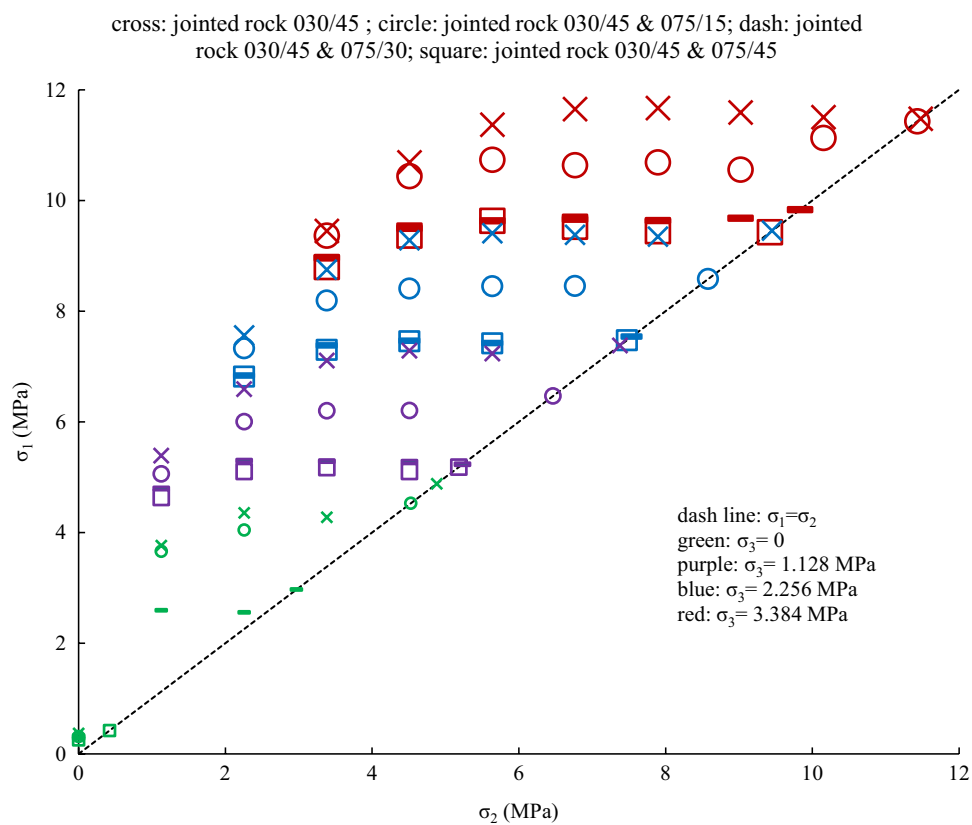


**Fig. 15** Polyaxial test results obtained from PFC<sup>3D</sup> modeling for the jointed rock model having three joints with 30° joint dip direction and 45° joint dip angle and the jointed rock models having six joints formed from two joint sets with 30° joint dip direction and 45° joint dip angle for the first joint set and 75° joint dip direction and the various joint dip angles from 15° to 45° at an interval of 15° for the second joint set



$$F_{ij} = \frac{1}{V} \sum_{i=1}^{m(V)} 2\pi r^3 n_i n_j \quad (4)$$

where  $F_{ij}^r$  is the fracture tensor of the rock mass,  $F_{ij}^k$  is the fracture tensor ( $F_{ij}$ ) of the  $k$ th joint set,  $N$  is the total number of joint sets,  $m(V)$  is the number of fracture centers inside the assumed volume of  $V$ , and  $n_i$  and  $n_j$  are the projection of  $\mathbf{n}$  on the directions of  $i$  and  $j$ , respectively. Table 6 shows the computed fracture tensor components for all 12 different joint systems with one or two joint sets which are modeled using the PFC<sup>3D</sup>. In this table because the maximum, intermediate and minimum principal stresses are applied in Z, Y and X directions, respectively, the alternate subscripts are also used to show the directions of the fracture tensor components with respect to the principal stresses.

Kulatilake et al. (2006) showed that for the biaxial loading in the laboratory on about 150 synthetic rock blocks having two joint sets with 30 different joint systems in which the joint set dip directions were towards the intermediate principal stress direction, the rock mass strength,  $\sigma_J$ , under a constant intermediate principal stress, reduces non-linearly with increasing fracture tensor component in the intermediate principal stress direction ( $F_{22}$ ). After trying various functions such as hyperbolic, negative power and negative exponential functions they proposed the following negative exponential equation which had the best regression fit to the experimental test results:

$$\frac{\sigma_J}{\sigma_I} = e^{-\lambda F_{22}} \quad (5)$$

In Eq. 5,  $\sigma_I$  is the intact rock strength under the same intermediate principal stress and  $\lambda$  is an empirical coefficient which is a function of  $\sigma_2$  according to Eq. 6.

$$\lambda = \frac{\lambda_0}{p \left( \frac{\sigma_2}{\sigma_c} \right)^q + 1}, \quad (6)$$

where  $\sigma_c$  is the uniaxial compressive strength of the intact rock,  $p$  and  $q$  are empirical coefficients and  $\lambda_0$  is the  $\lambda$  value when the intermediate principal stress equals to zero.

Later He et al. (2016) extended the Kulatilake et al. (2006) criterion to the polyaxial compressive stress condition by Eq. 7 based on extensive laboratory and numerical polyaxial test results on jointed coal blocks. In Eq. 7,  $F_{33}$  is the fracture tensor component in the minimum principal stress direction.

$$\frac{\sigma_J}{\sigma_I} = e^{-\lambda(F_{22} + F_{33})}. \quad (7)$$

They also proposed Eq. 8 for  $\lambda$  to incorporate the effect of the minimum principal stress,  $\sigma_3$ , as well as the intermediate principal stress. Like Eq. 6,  $\lambda_0$  is the  $\lambda$  value for the uniaxial compression condition.

$$\lambda = \frac{\lambda_0}{p_2 \left( \frac{\sigma_2}{\sigma_c} \right)^{q_2} + p_3 \left( \frac{\sigma_3}{\sigma_c} \right)^{q_3} + 1}, \quad (8)$$

where  $p_2$ ,  $q_2$ ,  $p_3$  and  $q_3$  are empirical coefficients.

This three-dimensional criterion can predict the strength of jointed rock masses under different confining stresses by estimating the five independent coefficients through regression analyses of the data. Procedures are given in He et al. (2016) in detail to do that. This criterion was developed for non-persistent fracture systems and it captures the effect of scale and anisotropy due to the fracture system on rock mass strength. The proposed criterion by He et al. (2016) can predict the rock mass strength reasonably accurately for non-persistent fracture systems. However, it can be extended to make it suitable for both non-persistent as well as persistent

**Table 6** The computed fracture tensor components in x, y, and z directions (the minimum, intermediate and maximum principal stress directions, respectively) for 12 joint systems of the jointed rock blocks

Joint system (Dip direction/Dip)	$F_{xx}$ ( $F_{33}$ )	$F_{yy}$ ( $F_{22}$ )	$F_{zz}$ ( $F_{11}$ )	$F_{xy}$ ( $F_{32}$ )	$F_{xz}$ ( $F_{31}$ )	$F_{yz}$ ( $F_{21}$ )
030/15	0.060	0.179	3.326	0.103	0.446	0.772
030/30	0.230	0.690	2.759	0.398	0.796	1.380
030/45	0.446	1.337	1.783	0.772	0.891	1.544
030/15 and 075/15	0.282	0.195	6.653	0.163	1.307	1.003
030/15 and 075/30	0.840	0.235	5.835	0.312	1.845	1.147
030/15 and 075/45	1.199	0.261	4.547	0.409	1.625	1.088
030/30 and 075/15	0.453	0.706	6.086	0.458	1.657	1.610
030/30 and 075/30	1.010	0.746	5.268	0.607	2.196	1.755
030/30 and 075/45	1.369	0.722	3.980	0.703	1.976	1.696
030/45 and 075/15	0.669	1.353	5.109	0.832	1.752	1.775
030/45 and 075/30	1.226	1.393	4.292	0.981	2.291	1.919
030/45 and 075/45	1.585	1.419	3.004	1.077	2.070	1.860

fracture systems. In He et al. (2016) criterion, for a set of constant values of the minimum and intermediate principal stresses  $\sigma_2$  and  $\sigma_3$ ,  $\lambda$  is a constant for a specified rock mass irrespective of the directions of  $\sigma_2$  and  $\sigma_3$ . When  $\sigma_2$  and  $\sigma_3$  directions rotate around the vector normal to the plane of  $\sigma_2$  and  $\sigma_3$  (i.e. in  $\sigma_1$  direction)  $F_{11}$  stays as a constant because the first invariant of the fracture tensor ( $F_{11} + F_{22} + F_{33}$ ) is always a constant and thus  $F_{22} + F_{33}$  also stays as a constant. Therefore, under the above-mentioned conditions, Eq. 7 provides a constant value and cannot capture the effect of  $\sigma_2$  on  $F_{22}$  and  $\sigma_3$  on  $F_{33}$  separately in predicting rock mass strength. However, this is an important issue to incorporate in predicting rock mass strength especially for persistent fracture systems.

In this research, Eqs. 7 and 8 are extended to capture the effect of  $\sigma_2$  on  $F_{22}$  and  $\sigma_3$  on  $F_{33}$  separately and to develop new rock mass strength criteria based on the results obtained through the jointed rock block modeling and testing under different minimum and intermediate stress combinations and joint geometry systems. The obtained results lead to the following observations:

- (a) Increase of joint set dip angles, in general, reduce the jointed rock block strength and increase  $F_{22}$  and  $F_{33}$ . Thus, increase of  $F_{22}$  and  $F_{33}$  reduce the jointed rock block strength.
- (b) Increase of the minimum and intermediate principal stresses reduce the effect of joint shearing on the jointed rock block strength. Therefore, increase of the minimum and intermediate principal stresses reduce the effects of  $F_{22}$  and  $F_{33}$ . However, this reduction for low minimum and intermediate principal stresses is relatively higher compared to high minimum and intermediate principal stresses.
- (c) The effect of the minimum principal stress on the joints increases with decreasing angle between the dip direction angle of the joint set and the minimum principal stress direction. Thus, increase of  $F_{33}$  increases the effect of  $\sigma_3$  on the joints.
- (d) The effect of the intermediate principal stress on the joints increases with decreasing angle between the dip direction angle of the joint set and the intermediate principal stress direction. Thus, increase of  $F_{22}$  increases the effect of  $\sigma_2$  on the joints.

Based on the above-mentioned observations the following equation is proposed as a new rock mass strength criterion in a general form.

$$S_r = \frac{\sigma_J}{\sigma_I} = \exp - [f_3(\sigma_3/\sigma_c)F_{33} + f_2(\sigma_2/\sigma_c)F_{22}], \quad (9)$$

where  $f_2$  and  $f_3$  are monotonically decreasing functions,  $S_r$  is the strength ratio between the jointed rock mass strength,  $\sigma_J$ ,

under the minimum and intermediate principal stresses of  $\sigma_3$  and  $\sigma_2$  and the intact rock strength,  $\sigma_I$ , under the same minimum and intermediate principal stresses,  $\sigma_c$  is the uniaxial compressive strength of the intact rock,  $F_{22}$  is the fracture tensor component in  $\sigma_2$  direction and,  $F_{33}$  is the fracture tensor component in  $\sigma_3$  direction. It should be mentioned that if  $\sigma_I$  for the intended  $\sigma_3$  and  $\sigma_2$  combination is not available, based on the Mehranpour and Kulatilake (2016) paper one of the three intact rock failure criteria out of Modified Lade, Modified Wiebols and Cook and Mogi is recommended to represent the intact rock strength value. However, because in this research the intact rock strength for all minimum and intermediate principal stress combinations is available, it is not necessary to use intact rock failure criteria to estimate the intact rock strength.

Kulatilake et al. (2006) showed that for the biaxial loading a function such as given by Eq. 6 works very well for  $f_2$  and  $f_3$ . Thus, Eq. 9 can be rewritten as follows to propose the first new rock mass strength criterion:

$$S_r = \frac{\sigma_J}{\sigma_I} = \exp - \left[ \frac{\lambda_3}{p_3 \left( \frac{\sigma_3}{\sigma_c} \right)^{q_3} + 1} F_{33} + \frac{\lambda_2}{p_2 \left( \frac{\sigma_2}{\sigma_c} \right)^{q_2} + 1} F_{22} \right], \quad (10)$$

where  $\lambda_2, \lambda_3, p_2, p_3, q_2$  and  $q_3$  are empirical coefficients. As an alternative, to reduce the number of coefficients, negative exponential functions are suggested for both  $f_2$  and  $f_3$ . Thus, Eq. 9 can be rewritten as Eq. 11 with less empirical coefficients to propose the second new rock mass strength criterion.

$$S_r = \frac{\sigma_J}{\sigma_I} = \exp - \left[ a_3 \left( e^{-b_3(\sigma_3/\sigma_c)} F_{33} \right) + a_2 \left( e^{-b_2(\sigma_2/\sigma_c)} F_{22} \right) \right], \quad (11)$$

where  $a_2, a_3, b_2$  and  $b_3$  are empirical coefficients.

It should be mentioned that if the joints have the same mechanical properties with isotropic behavior on the joint plane, the effect of  $\sigma_2$  variation on  $F_{22}$  should be the same as the effect of  $\sigma_3$  variation on  $F_{33}$ . Therefore, under this condition  $f = f_2 = f_3$  and Eqs. 9–11 can be simplified to Eqs. 12–14, respectively, as follows:

$$S_r = \frac{\sigma_J}{\sigma_I} = \exp - [f(\sigma_3/\sigma_c)F_{33} + f(\sigma_2/\sigma_c)F_{22}], \quad (12)$$

$$S_r = \frac{\sigma_J}{\sigma_I} = \exp - \lambda \left[ \frac{F_{33}}{p \left( \frac{\sigma_3}{\sigma_c} \right)^q + 1} + \frac{F_{22}}{p \left( \frac{\sigma_2}{\sigma_c} \right)^q + 1} \right], \quad (13)$$

$$S_r = \frac{\sigma_J}{\sigma_I} = \exp - a \left[ \left( e^{-b(\sigma_3/\sigma_c)} F_{33} \right) + \left( e^{-b(\sigma_2/\sigma_c)} F_{22} \right) \right]. \quad (14)$$

In Eq. 12,  $f$  is a monotonically decreasing function and in Eqs. 13 and 14,  $\lambda$ ,  $p$ ,  $q$ ,  $a$  and  $b$  are empirical coefficients. Moreover, under this condition if  $\sigma_2 = \sigma_3$ , by rotating the  $\sigma_2$  and  $\sigma_3$  directions around the vector normal to the plane of  $\sigma_2$  and  $\sigma_3$ , the jointed rock mass strength should remain the same. This behavior is also captured by Eq. 12. If  $\sigma_2 = \sigma_3$ , Eq. 12 can be rewritten as follows:

$$S_r = \frac{\sigma_J}{\sigma_I} = \exp - [f(\sigma_3/\sigma_c)(F_{33} + F_{22})], \quad (15)$$

where  $F_{33} + F_{22}$  is always a constant if  $\sigma_2$  and  $\sigma_3$  directions rotate around the vector normal to the plane of  $\sigma_2$  and  $\sigma_3$ . Therefore, the jointed rock mass strength stays the same under the above-mentioned conditions.

In this research because all the joints are saw cut, they have the same isotropic mechanical behavior on the joint plane. Thus, to fit the new rock mass strength criteria for the numerical modeling results and to find the accuracy of the new rock mass strength criteria Eqs. 13 and 14 can be used. To estimate the values of the coefficients in these equations an indirect method is used. In this method, different values are chosen for empirical coefficients from a grid in a reasonable range. Then the jointed rock mass strength corresponding to different  $\sigma_2$ ,  $\sigma_3$ ,  $F_{22}$  and  $F_{33}$  values are calculated through Eqs. 13 and 14. Afterwards, for each equation the best combination of the empirical coefficients is found by maximizing the coefficient of determination,  $R^2$ , using the following equations:

$$R^2 = 1 - \frac{S_e}{S_t}, \quad (16)$$

where

$$S_e = \frac{1}{n-m-1} \sum_{i=1}^n \left( \sigma_{J,i}^P - \bar{\sigma}_J^P \right)^2, \quad (17)$$

$$S_t = \frac{1}{n-1} \sum_{i=1}^n \left( \sigma_{J,i}^P - \bar{\sigma}_J^P \right)^2, \quad (18)$$

where  $n$  is the total number of data sets,  $m$  is the number of parameters to be estimated,  $\sigma_{J,i}^P$  is the predicted jointed rock block strength from the new rock mass strength criterion for data set  $i$ ,  $\sigma_{J,i}^P$  is the strength of jointed rock block from the PFC<sup>3D</sup> modeling for data set  $i$ , and  $\bar{\sigma}_J^P$  is the average strength value of all the PFC<sup>3D</sup> data.

#### 4.1 Fitting of the First New Rock Mass Strength Criterion Using Eq. 13

In Fig. 16, the obtained  $R^2$  values are shown for different values of  $p$  and  $q$  for selected 3 different  $\lambda$  values. The maximum  $R^2$  is found to be 0.94, indicating a very strong fit. It results in the best values of 0.675, 3.16 and 0.6, for  $\lambda$ ,  $p$  and  $q$ , respectively. Figure 17 shows the predicted strength values versus the strength values from the PFC<sup>3D</sup> modeling for all 284 data points. It indicates that the suggested strength criterion (Eq. 13) is highly suitable to represent the PFC<sup>3D</sup> data.

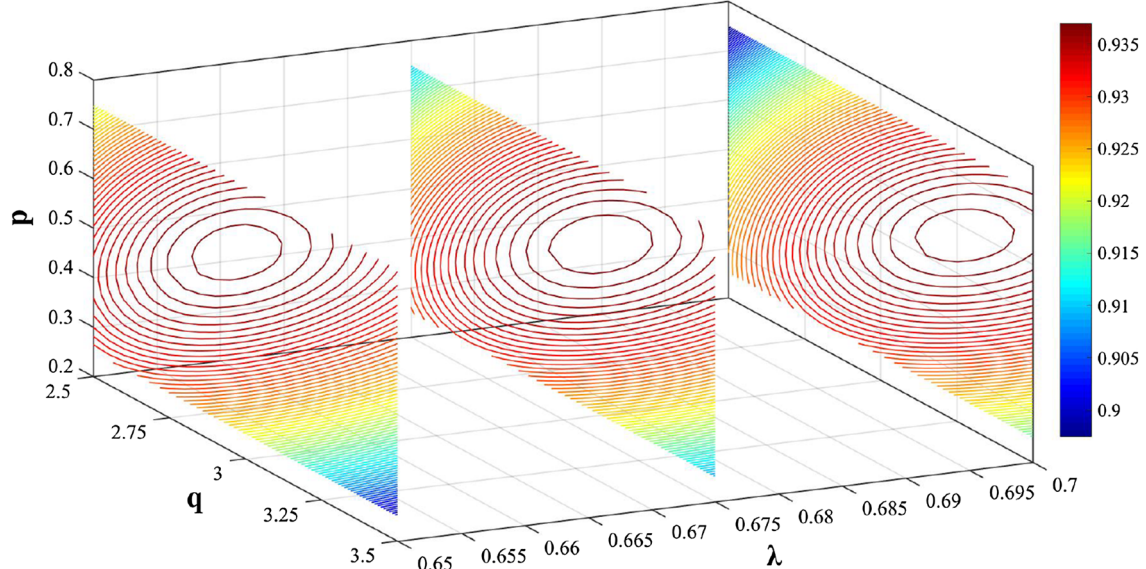


**Fig. 16** Obtained  $R^2$  values of the new rock mass strength criterion using Eq. 13 for different combinations of  $p$ ,  $q$  on the cross-sectional planes of  $\lambda=0.65$ ,  $\lambda=0.675$  and  $\lambda=0.70$  (color bar shows the  $R^2$  values)

**Fig. 17** Predicted strength values based on the new rock mass strength criterion based on Eq. 13 versus the strength values from PFC<sup>3D</sup> modeling for all 284 data points from 12 different joint systems having different boundary conditions ( $R^2=0.94$ )

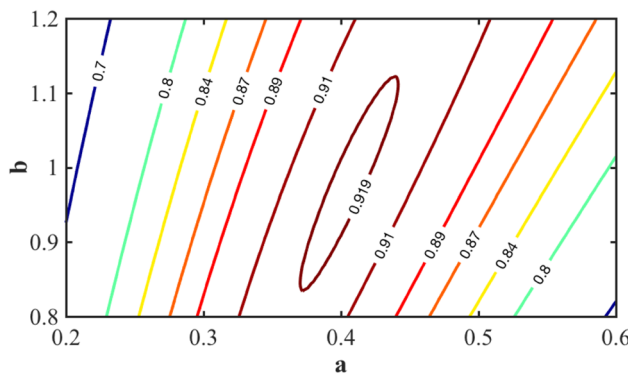
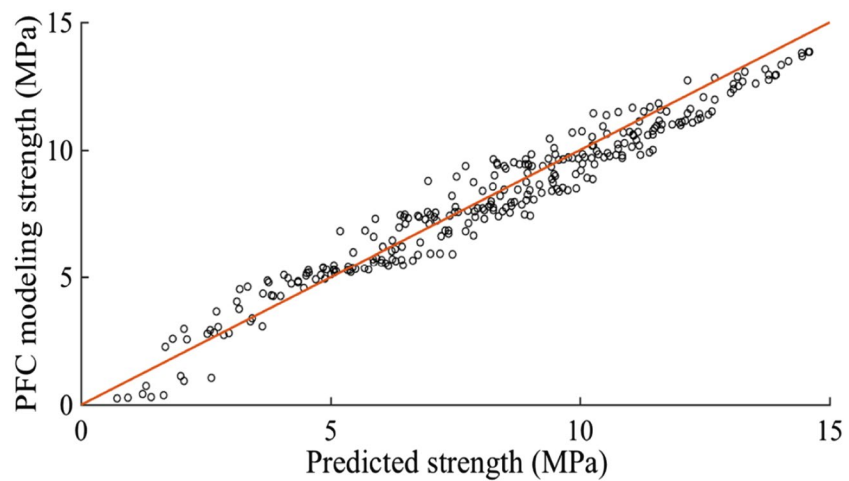


**Fig. 18** Obtained  $R^2$  values of the new rock mass strength criterion using Eq. 14 for different combinations of  $a$  and  $b$

#### 4.2 Fitting of the Second New Rock Mass Strength Criterion Using Eq. 14

In Fig. 18, the obtained  $R^2$  values are shown for different values of  $a$  and  $b$  for the 284 data points from 12 different joint systems under the different minimum and intermediate principal stress combinations. The maximum  $R^2$  is found to be 0.92. It results in the best values of 0.404 and 0.972, for  $a$  and  $b$ , respectively. The small difference obtained between the  $R^2$  values using the two different functions shows that Eq. 14 with less empirical coefficients is also a reasonably good rock mass strength criterion. Figure 19 shows the predicted strength values based on Eq. 14 versus the strength values from the PFC<sup>3D</sup> modeling for all 284 data points. It indicates that the suggested strength criterion (Eq. 14) is highly suitable to represent the PFC<sup>3D</sup> data. Figure 20 shows the comparison between the predicted rock mass strengths from the new rock mass strength criteria using Eqs. 13 and 14 with the numerical results for two different joint systems with one and two joint sets, respectively. Figure 20 shows that the predictions from the two strength criteria are close.

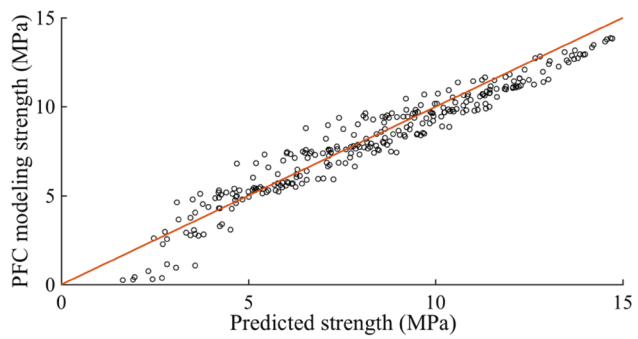
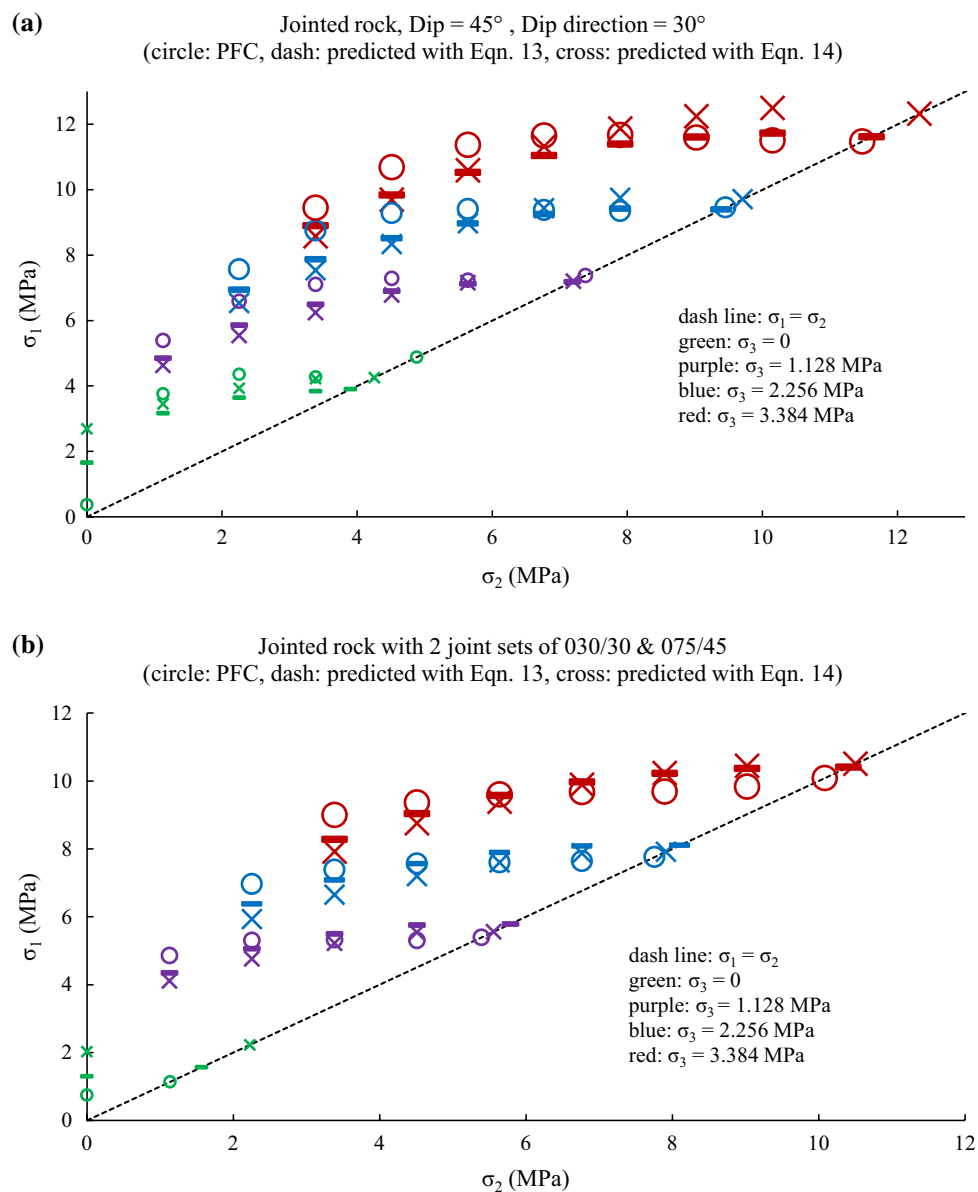


**Fig. 19** Predicted strength value based on the new rock mass strength criterion using Eq. 14 versus the strength value from PFC<sup>3D</sup> for all 284 data points from 12 different joint systems and under different boundary conditions ( $R^2=0.92$ )

## 5 Discussion

The equations given in Sect. 4 to estimate the jointed block strength for synthetic rock are normalized with respect to the synthetic intact rock strength. Therefore, the equations are applicable for any rock mass. The equations allow to estimate the normalized jointed block strength in any direction in three dimensions. By estimating the strength in different directions, the strength anisotropy and the minimum normalized jointed block strength can be estimated in three dimensions. The intact block strength can be estimated using one of the available intact rock strength criteria. To estimate the parameters of the intact rock strength criterion, it will be necessary to perform a few laboratory tests as usual. To apply the equations given for normalized jointed block strength for any rock mass, first, the fracture geometry data (number of fracture sets and orientation, size and intensity of each set) should be collected for the intended rock mass. These data can be used to calculate the fracture tensor using Eqs. 3 and 4 as shown in Table 6. That will allow calculation

**Fig. 20** Comparison of the pol-axial strength results obtained from the PFC<sup>3D</sup> modeling with that obtained from the new rock mass strength criteria based on Eqs. 13 and 14, respectively, for the jointed rock block models **a** having 3 joints with dip angle and dip direction of 45° and 30°, respectively, and **b** having six joints formed from two joint sets with 30° joint dip direction and 30° joint dip angle for the first joint set and 75° joint dip direction and 45° joint dip angle for the second joint set



of the two fracture tensor components perpendicular to the direction jointed block strength is desired. These two fracture tensor components go into the normalized jointed block strength equation. The confining stresses should be applied based on the in-situ stress system. For the time being the estimated coefficient values of the equations can be used to estimate the jointed block strength. It is important to note that these coefficient values depend on the ratios of joint mechanical property values to intact rock property values. This dependence should be investigated in future research.

## 6 Summary and Conclusions

In this research an attempt was made to develop a new three-dimensional rock mass strength criterion to overcome the shortcomings that exist in most of the existing rock mass strength criteria. Most of the existing strength criteria cannot simultaneously consider the effect of the intermediate principal stress on the rock mass strength as well as the scale dependency and anisotropy behavior of the rock mass strength. Although He et al. (2016) proposed a three-dimensional criterion which captures the effect of the intermediate principal stress, scale dependency and anisotropy due to the fracture system on rock mass strength their criterion did not incorporate the effect of the stress anisotropy because it was developed for non-persistent fracture systems. Besides, He

et al. (2016) criterion requires calibration of five empirical coefficients. However, the stress anisotropy is important especially in the case of fully persistent fracture systems (Mehrani and Kulatilake 2017). Therefore, in this paper the He et al. (2016) criterion was extended to incorporate the effect of stress anisotropy too and to develop two new rock mass strength criteria.

To develop a comprehensive rock mass strength criterion, it is crucial to have a proper database which includes the effect of different factors such as the joint geometry configuration including the orientation and the minimum and intermediate principal stresses. Due to the high cost and time of the experimental tests, it is very difficult if not impractical to have a comprehensive database only through experimental tests. Therefore, numerical modeling was incorporated to create this database. The other benefit of the numerical modeling is the possibility to investigate the effect of each factor separately while keeping the values of the other factors the same. In this research, PFC<sup>3D</sup> was selected for the numerical modeling because it can conveniently model the block breakage through the fracture initiation and propagation using the Bonded Particle Models and joint failure through the joint sliding using the SJCM. In this paper, because of the shortcoming of the SJCM to capture the non-linear behavior of the joint closure due to varying joint normal stress, the MSJCM was used. Moreover, to solve the interlocking problem which occurs due to the shortcoming of the PFC software in the updating procedure of the contact conditions of the particles that lie around the intended joint plane during high shear displacements, the JSC approach was used.

Before simulating the jointed rock blocks under the polyaxial, triaxial and biaxial compression tests, these tests were simulated on the synthetic intact rock samples to find the intact rock strength for selected minimum and intermediate principal stress combinations. Altogether 33 intact rock strength values for different combinations of minimum and intermediate principal stresses were obtained from the numerical modeling for the synthetic intact rock. Then, 12 different joint systems with one and two joint sets were chosen to model the jointed rock blocks under the polyaxial, triaxial and biaxial compression tests with the minimum and intermediate principal stress combinations similar to those conducted for the intact rock modeling. Used joint sets have different dip angles varying from 15° to 45° at an interval of 15° with dip directions of 30° and 75°. Each joint set also has three persistent joints with the joint spacing of 42 mm in a cubic sample of size 160 mm. In total 284 jointed block strengths were obtained from the numerical modeling of the jointed rock blocks. It should be mentioned that because the numerical and experimental test results of polyaxial and triaxial compression tests on the synthetic intact rock and jointed rock blocks showed a reasonable agreement, it was

not necessary to update the micro mechanical properties of the calibrated PFC<sup>3D</sup> model.

Based on the observations from the jointed rock modeling results using PFC<sup>3D</sup> and the fracture tensor concept, an existing rock mass strength criterion was extended to include the stress anisotropy and to develop a new three-dimensional rock mass strength criterion in general form (Eq. 9). For the new general rock mass strength criterion, two functions were proposed: (a) given by Eq. 10 and (b) given by Eq. 11 to obtain two specific new rock mass strength criteria. The new rock mass strength criterion given by Eq. 10 has six empirical coefficients; if the joint sets have the same isotropic mechanical behavior on the joint plane, the number of coefficients reduces to three empirical coefficients in this criterion (Eq. 13). The new rock mass strength criterion given by Eq. 11 has only four empirical coefficients; if the joint sets have the same isotropic mechanical behavior on the joint plane the number of coefficients reduces to two empirical coefficients in this criterion (Eq. 14).

Using the database created in this paper, which has 284 data points, the empirical coefficients of  $\lambda$ ,  $p$  and  $q$  were estimated as 0.675, 3.16 and 0.6, respectively, through a grid analysis with a high  $R^2$  value of 0.94 for the new criterion given by Eq. 13. The empirical coefficients of  $a$  and  $b$  were estimated as 0.404 and 0.972, respectively, through a grid analysis with a high  $R^2$  value of 0.92 for the new criterion given by Eq. 14. Even though the first criterion was fitted with a slightly higher  $R^2$  value than the second criterion, it was less time consuming and significantly easier to estimate the empirical coefficients for the second criterion. Both new criteria clearly showed the effect of the intermediate principal stress as well as the minimum principal stress and joint orientation on the rock mass strength. Because the developed jointed block strength criteria are expressed in normalized form by dividing by the intact block strength, the normalized jointed block strength criteria are applicable for any rock mass. Guidelines are given to show how the developed strength criteria can be applied to field rock masses.

**Acknowledgements** The research was funded by the National Institute for Occupational Safety, and Health (NIOSH) of the Centers for Disease Control, and Prevention (Contract No. 200-2011-39886).

## References

- Amadei B (1996) Importance of anisotropy when estimating and measuring in situ stresses in rock. *Int J Rock Mech Min Sci* 33(3):293–325. [https://doi.org/10.1016/0148-9062\(95\)00062-3](https://doi.org/10.1016/0148-9062(95)00062-3)
- Bahaaddini M, Sharrock G, Hebblewhite BK (2013) Numerical direct shear tests to model the shear behaviour of rock joints. *Comput Geotech* 51:101–115. <https://doi.org/10.1016/j.compgeo.2013.02.003>
- Bahaaddini M, Hagan PC, Mitra R, Hebblewhite BK (2015) Parametric study of smooth joint parameters on the shear behaviour of

rock joints. *Rock Mech Rock Eng* 48(3):923–940. <https://doi.org/10.1007/s00603-014-0641-6>

Bandis SC, Lumsden AC, Barton NR (1983) Fundamentals of rock joint deformation. *Int J Rock Mech Min Sci Geomech* 20(6):249–268. [https://doi.org/10.1016/0148-9062\(83\)90595-8](https://doi.org/10.1016/0148-9062(83)90595-8)

Barton N, Lien R, Lunde J (1974) Engineering classification of rock masses for the design of tunnel support. *Rock Mech Rock Eng* 6(4):189–236. <https://doi.org/10.1007/BF01239496>

Bekaert A, Maghous S (1996) Three-dimensional yield strength properties of jointed rock mass as a homogenized medium. *Mech Cohes-Frict Mat* 1(1):1–24. [https://doi.org/10.1002/\(SICI\)1099-1484\(199601\)1:1%3C1::AID-CFM1%3E3.0.CO;2-O](https://doi.org/10.1002/(SICI)1099-1484(199601)1:1%3C1::AID-CFM1%3E3.0.CO;2-O)

Bieniawski ZT (1973) Engineering classification of jointed rock masses. *Trans S Afr Inst Civ Eng* 15:335–344

Chiu CC, Wang TT, Weng MC, Huang TH (2013) Modeling the anisotropic behavior of jointed rock mass using a modified smooth-joint model. *Int J Rock Mech Min Sci* 62:14–22. <https://doi.org/10.1016/j.ijrmms.2013.03.011>

Cho NA, Martin CD, Sego DC (2007) A clumped particle model for rock. *Int J Rock Mech Min Sci* 44(7):997–1010. <https://doi.org/10.1016/j.ijrmms.2007.02.002>

Colak K, Unlu T (2004) Effect of transverse anisotropy on the Hoek–Brown strength parameter ‘ $m$ ’ for intact rocks. *Int J Rock Mech Min Sci* 41(6):1045–1052. <https://doi.org/10.1016/j.ijrmms.2004.04.004>

Cundall PA, Hart RD (1992) Numerical modelling of discontinua. *Eng computations* 9(2):101–113. <https://doi.org/10.1108/eb023851>

Cundall PA, Strack OD (1979) A discrete numerical model for granular assemblies. *Geotechnique* 29(1):47–65

Duan K, Kwok CY (2016) Evolution of stress-induced borehole breakout in inherently anisotropic rock: Insights from discrete element modeling. *J Geophys Res Solid Earth* 121(4):2361–2381. <https://doi.org/10.1002/2015JB012676>

Fakhimi A (2004) Application of slightly overlapped circular particles assembly in numerical simulation of rocks with high friction angles. *Eng Geol* 74(1):129–138. <https://doi.org/10.1016/j.enggeo.2004.03.006>

Fan X, Kulatilake PHSW, Chen X (2015) Mechanical behavior of rock-like jointed blocks with multi-non-persistent joints under uniaxial loading: a particle mechanics approach. *Eng Geol* 190:17–32. <https://doi.org/10.1016/j.enggeo.2015.02.008>

Gigli G, Casagli N (2011) Semi-automatic extraction of rock mass structural data from high resolution LIDAR point clouds. *Int J Rock Mech Min Sci* 48(2):187–198. <https://doi.org/10.1016/j.ijrmms.2010.11.009>

Goodman RE (1976) Methods of geological engineering in discontinuous rocks. West Information Publishing Group

He PF, Kulatilake PHSW, Liu DQ, He MC (2016) Development of a new three-dimensional coal mass strength criterion. *Int J Geomech* 17(3):04016067. [https://doi.org/10.1061/\(ASCE\)GM.1943-5622.0000741](https://doi.org/10.1061/(ASCE)GM.1943-5622.0000741)

Hoek E (1994) Strength of rock and rock masses. *ISRM News J* 2(2):4–16

Ismael MA, Imam HF, El-Shayeb Y (2014) A simplified approach to directly consider intact rock anisotropy in Hoek–Brown failure criterion. *J Rock Mech Geot Eng* 6(5):486–492. <https://doi.org/10.1016/j.jrmge.2014.06.003>

Itasca Consulting Group Inc (2016) PFC manual, version 5.0, Minneapolis

Koyama T, Jing L (2007) Effects of model scale and particle size on micro-mechanical properties and failure processes of rocks—a particle mechanics approach. *Eng Anal Bound Elem* 31(5):458–472. <https://doi.org/10.1016/j.enganabound.2006.11.009>

Kulatilake PHSW (1985) Estimating elastic constants and strength of discontinuous rock. *J Geotech Eng ASCE* 111(7):847–864. [https://doi.org/10.1061/\(ASCE\)0733-9410\(1985\)111:7\(847\)](https://doi.org/10.1061/(ASCE)0733-9410(1985)111:7(847)

Kulatilake PHSW (2016) Physical, empirical and numerical modeling of jointed rock mass strength. In: Feng XT, Hudson J (eds) *Rock Mechanics and Engineering*, CRC Press, Balkema (invited book chapter)

Kulatilake PHSW, Shu B (2015) Prediction of rock mass deformations in three dimensions for a part of an open pit mine and comparison with field deformation monitoring data. *Geotech Geol Eng* 33:1551–1568. <https://doi.org/10.1007/s10706-015-9921-5>

Kulatilake PHSW, Wang S, Stephansson O (1993) Effect of finite size joints on deformability of jointed rock at the three dimensional level. *Int J Rock Mech Min Sci* 30(5):479–501. [https://doi.org/10.1016/0148-9062\(93\)92216-D](https://doi.org/10.1016/0148-9062(93)92216-D)

Kulatilake PHSW, Malama B, Wang J (2001) Physical and particle flow modeling of jointed rock block behavior under uniaxial loading. *Int J Rock Mech Min Sci* 38(5):641–657. [https://doi.org/10.1016/S1365-1609\(01\)00025-9](https://doi.org/10.1016/S1365-1609(01)00025-9)

Kulatilake PHSW, Park J, Malama B (2006) A new rock mass failure criterion for biaxial loading conditions. *Geotech Geol Eng* 24(4):871–888. <https://doi.org/10.1007/s10706-005-7465-9>

Kulatilake PHSW, Shreedharan S, Sherizadeh T, Shu B, Xing Y, He P (2016) Laboratory estimation of rock joint stiffness and frictional parameters. *Geotech Geol Eng* 34(6):1723–1735. <https://doi.org/10.1007/s10706-016-9984-y>

Lee H, Jeon S (2011) An experimental and numerical study of fracture coalescence in pre-cracked specimens under uniaxial compression. *Int J Solids Struct* 48:979–999. <https://doi.org/10.1016/j.ijsolstr.2010.12.001>

Malama B, Kulatilake PHSW (2003) Models for normal fracture deformation under compressive loading. *Int J Rock Mech Min Sci* 40(6):893–901. [https://doi.org/10.1016/S1365-1609\(03\)00071-6](https://doi.org/10.1016/S1365-1609(03)00071-6)

Marinos V, Marinos P, Hoek E (2005) The geological strength index: applications and limitations. *Bull Eng Geol Environ* 64(1):55–65. <https://doi.org/10.1007/s10064-004-0270-5>

Mas Ivars D, Pierce ME, Darcel C, Reyes-Montes J, Potyondy DO, Young RP, Cundall PA (2011) The synthetic rock mass approach for jointed rock mass modelling. *Int J Rock Mech Min Sci* 48(2):219–244. <https://doi.org/10.1016/j.ijrmms.2010.11.014>

Mehranpour MH, Kulatilake PHSW (2016) Comparison of six major intact rock failure criteria using a particle flow approach under true-triaxial stress condition. *Geomech Geophy Geo-energ Georesour* 2(4):203–229. <https://doi.org/10.1007/s40948-016-0030-6>

Mehranpour MH, Kulatilake PHSW (2017) Improvements for the smooth joint contact model of the particle flow code and its applications. *Comput Geotech* 87:163–177. <https://doi.org/10.1016/j.compgeo.2017.02.012>

Melkoumian N, Priest SD, Hunt SP (2009) Further development of the three-dimensional Hoek–Brown yield criterion. *Rock Mech Rock Eng* 42(6):835–847. <https://doi.org/10.1007/s00603-008-0022-0>

Oda M (1982) Fabric tensor for discontinuous geological materials. *Soils Found* 22(4):96–108. [https://doi.org/10.3208/sandf.1972.22.4\\_96](https://doi.org/10.3208/sandf.1972.22.4_96)

Oda M (1984) Similarity rule of crack geometry in statistically homogeneous rock masses. *Mech Mater* 3(2):119–129. [https://doi.org/10.1016/0167-6636\(84\)90003-6](https://doi.org/10.1016/0167-6636(84)90003-6)

Pan XD, Hudson JA (1988) A simplified three dimensional Hoek–Brown yield criterion. In: ISRM International symposium. International Society for Rock Mechanics

Park JW, Song JJ (2009) Numerical simulation of a direct shear test on a rock joint using a bonded-particle model. *Int J Rock Mech Min Sci* 46(8):1315–1328. <https://doi.org/10.1016/j.ijrmms.2009.03.007>

Pierce M, Cundall P, Potyondy D, Mas Ivars D (2007) A synthetic rock mass model for jointed rock. In: Eberhardt E, Stead D, Morrison T (eds) *Rock Mechanics: Meeting Society’s Challenges and Demands. Proceeding of the 1st Canada–US rock mechanics*

symposium; May 27–31 Vancouver, Canada. London: Taylor & Francis Group, 1:341–349

Potyondy DO (2015) The bonded-particle model as a tool for rock mechanics research and application: current trends and future directions. *Geosyst Eng* 18(1):1–28. <https://doi.org/10.1080/12269328.2014.998346>

Potyondy DO, Cundall PA (2004) A bonded-particle model for rock. *Int J Rock Mech Min Sci* 41(8):1329–1364. <https://doi.org/10.1016/j.ijrmms.2004.09.011>

Pouya A, Ghoreychi M (2001) Determination of rock mass strength properties by homogenization. *Int J Numer Anal Met* 25(13):1285–1303. <https://doi.org/10.1002/nag.176>

Priest SD (2005) Determination of shear strength and three-dimensional yield strength for the Hoek–Brown criterion. *Rock Mech Rock Eng* 38(4):299–327. <https://doi.org/10.1007/s00060-005-0056-5>

Ramamurthy T (2001) Shear strength response of some geological materials in triaxial compression. *Int J Rock Mech Min* 38(5):683–697. [https://doi.org/10.1016/S1365-1609\(01\)00035-1](https://doi.org/10.1016/S1365-1609(01)00035-1)

Saroglou H, Tsiambaos G (2008) A modified Hoek–Brown failure criterion for anisotropic intact rock. *Int J Rock Mech Min* 45(2):223–234. <https://doi.org/10.1016/j.ijrmms.2007.05.004>

Schöpfer MP, Childs C, Manzocchi T (2013) Three-dimensional failure envelopes and the brittle-ductile transition. *J Geophys Res-Sol Ea* 118(4):1378–1392. <https://doi.org/10.1002/jgrb.50081>

Shehata WM (1972) fundamental considerations on the hydraulic characteristics of joints in rock. In: Proceedings of the symposium on percolation through fissured rock, Sep 18–19; Stuttgart, Germany. paper (No. T1-F)

Sheorey PR, Biswas A, Choubey VD (1989) An empirical failure criterion for rocks and jointed rock masses. *Eng Geol* 26(2):141–159. [https://doi.org/10.1016/0013-7952\(89\)90003-3](https://doi.org/10.1016/0013-7952(89)90003-3)

Shreedharan S, Kulatilake PHSW (2016) Discontinuum-equivalent continuum analysis of the stability of tunnels in a deep coal mine using the distinct element method. *Rock Mech Rock Eng* 49(5):1903–1922. <https://doi.org/10.1007/s00060-015-0885-9>

Singh B, Goel RK (2011) Engineering rock mass classification: tunnelling, foundations and landslides. Butterworth-Heinemann (an imprint of Elsevier), Massachusetts

Swan G (1983) Determination of stiffness and other joint properties from roughness measurements. *Rock Mech Rock Eng* 16(1):19–38. <https://doi.org/10.1007/BF01030216>

Wu Q, Kulatilake PHSW (2012) REV and its properties on fracture system and mechanical properties, and an orthotropic constitutive model for a jointed rock mass in a dam site in China. *Comput Geotech* 43:124–142. <https://doi.org/10.1016/j.compgeo.2012.02.010>

Yang X, Kulatilake PHSW, Jing H, Yang S (2015) Numerical simulation of a jointed rock block mechanical behavior adjacent to an underground excavation and comparison with physical model test results. *Tunn Undergr Sp Tech* 50:129–142. <https://doi.org/10.1016/j.tust.2015.07.006>

Yu Q (2001) Computational simulations of shear behavior of joints in brittle geomaterials. Doctoral dissertation, McGill University, Montreal

Yudhbir Y, Lemanza W, Prinzl F (1983) An empirical failure criterion for rock masses. In 5th ISRM Congress. International Society for Rock Mechanics

Zhang L (2008) A generalized three-dimensional Hoek–Brown strength criterion. *Rock Mech Rock Eng* 41(6):893–915. <https://doi.org/10.1007/s00060-008-0169-8>

Zhang L, Zhu H (2007) Three-dimensional Hoek–Brown strength criterion for rocks. *J Geotech Geoenvir* 133(9):1128–1135. [https://doi.org/10.1061/\(ASCE\)1090-0241\(2007\)133:9\(1128](https://doi.org/10.1061/(ASCE)1090-0241(2007)133:9(1128)

Zhang Q, Zhu H, Zhang L (2013) Modification of a generalized three-dimensional Hoek–Brown strength criterion. *Int J Rock Mech Min* 59:80–96. <https://doi.org/10.1016/j.ijrmms.2012.12.009>

Zhang Y, Stead D, Elmo D (2015) Characterization of strength and damage of hard rock pillars using a synthetic rock mass method. *Comput Geotech* 65:56–72. <https://doi.org/10.1016/j.compgeo.2014.12.002>

Zheng J, Kulatilake PHSW, Shu B, Sherizadeh T, Deng J (2014) Probabilistic block theory analysis for a rock slope at an open pit mine in USA. *Comput Geotech* 61:254–265. <https://doi.org/10.1016/j.compgeo.2014.06.002>

**Publisher's Note** Springer Nature remains neutral with regard to jurisdictional claims in published maps and institutional affiliations.